

Chapter 4 CO oxidation over O-rich phases on Ru(0001)

4.1 Motivation

At sample temperatures above 500 K, additional NO₂ or O₂ exposures to the (1×1)-O phase lead to a further uptake of oxygen [23, 25]. The existence of O-rich phases can be verified with thermal desorption experiments. The O phases with O coverages below 1.0 ML show desorption peaks between 1100 K and 1600 K, exhibiting second-order desorption [23]. The TD spectra of the O-rich phases with O coverages above 1.0 ML show an additional peak at about 1000 K [23, 44–46]. With increasing O coverage, this additional thermal desorption state grows in intensity, but its peak temperature does not shift. This is a characteristic for the first-order desorption.

Most of the previous studies used NO₂ to prepare the O-rich phases [25, 44, 45]. The properties of the O-rich phases were studied by using the techniques of XPS, UPS, LEED, and TDS [25, 44, 45].

XPS studies have shown that no oxide structure develops, until O coverage reaches 40 ML [44, 45]. LEED patterns of O-rich phases did not show any indication of the oxide formation, although the O coverage was much higher than 1 ML [25]. From the LEED I/E analysis no additional O atoms between the first and second layer were found, although the existence of additional O atoms beside the (1×1)-O overlayer was evidenced by thermal desorption experiments [25]. The authors concluded that the O atoms are distributed in deeper bulk layers rather than staying in the subsurface region.

The bottom line of all these investigations is that the O-rich phases with O coverages between 1 ML to 10 ML prepared with NO₂ do not indicate any oxide formation on the surface. Just the (1×1)-O was found on Ru(0001), while additional O atoms were suggested to be below the surface. The position of these O atoms below the surface is, however, not yet clear.

The study of O-rich phases of Ru(0001) became attractive due to their high

activity for CO oxidation [23, 24]. It has to be emphasized that O₂ instead of NO₂ was used in Ref. [23, 24] for the preparation of the O-rich phases.

The probability of CO to CO₂ conversion of the (1×1)-O on Ru(0001) turned out to be about 0.01 % [23]. The (1×1)-O lattice does not allow adsorption of CO above 50 K. Therefore, the CO oxidation proceeds only via O vacancies. Quite in contrast, titration measurements revealed that the probability of CO to CO₂ conversion increases to 1 %, when the initial O coverage on Ru(0001) is 7.3 ML [23]. It was shown that the CO to CO₂ conversion probability increases dramatically, when the O coverage exceeds 2–3 ML. Subsurface O atoms were suggested to play an important role for the high activity towards CO oxidation.

This conclusion was based on a comparison with the results obtained for the O-rich phases prepared by NO₂ exposures. It was assumed by the authors of Ref. [23] that the preparations with O₂ and NO₂ lead to identical O phases, as long as the O coverage is the same. It was supposed that the active O-rich phases prepared by using O₂ consist of the (1×1)-O overlayer and subsurface O atoms.

A recent molecular beam experiment showed that the diffusion of O atoms from deeper layers towards the surface is an important reaction channel in the CO oxidation over the O-rich Ru(0001) surfaces [24]. In Fig. 4.1, the results of these experiments are summarized [24]. The CO-molecular beams were directed to the Ru(0001) surfaces, which were precovered with an initial O coverage of 16 ML. The outgoing CO₂ signals were recorded in the specula direction as a function of reaction time. The sample temperature was varied from 300 K to 675 K.

The CO₂ traces versus titration time (Fig. 4.1) consist of a fast component and a slow component. The fast component appears at the beginning of each measurement. The slow component starts to appear, after the fast component signal declines. The signal of the slow component can be observed for several hundred seconds. At sample temperatures between 300 K and 450 K, just the fast component is detectable. The slow component appears at sample temperatures above 500 K. At lower sample temperatures, O diffusion towards the surface is not allowed for

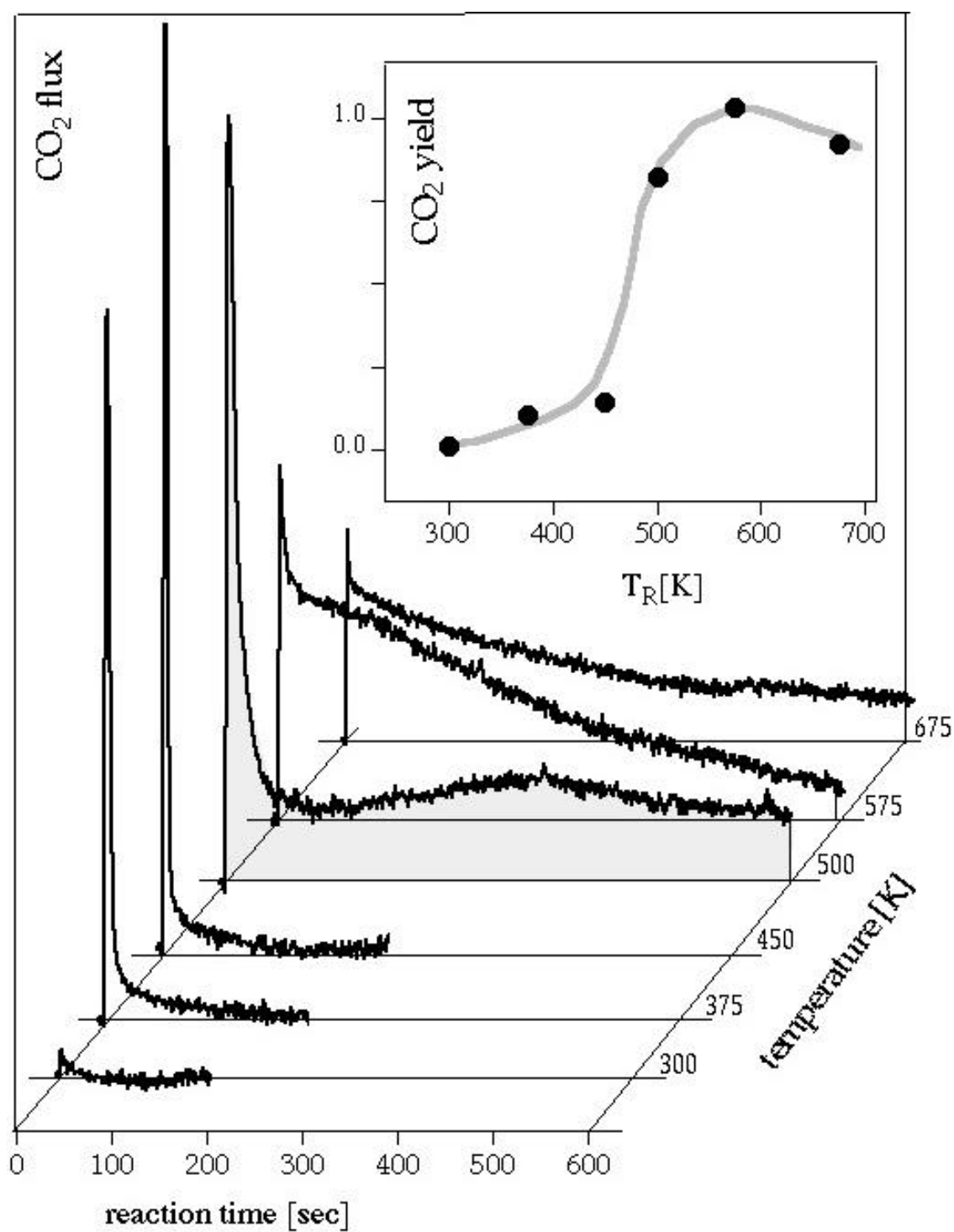


Fig. 4.1. CO₂ flux caused by a CO-molecular beam striking O-precovered Ru(0001) surfaces at various sample temperatures [24]. The initial O coverage was 16 ML. The integral of each spectrum (total CO₂ yield) is shown in the inset.

kinetic reasons. Thus, only the O atoms on the surface are able to react with CO. The fast component is caused by the reaction between CO and O on the surface. At higher temperatures, the diffusion barrier of O can be overcome. The slow component arises from the reaction between CO and O, which arrived from deeper layers by diffusion.

From the used chopper frequency of 160 MHz, the residence time of CO on the surface could be estimated to be larger than 1 ms at sample temperatures between 450 K and 575 K. Apparently, the CO oxidation takes place via the Langmuir-Hinshelwood mechanism [24]. Thermal desorption experiments showed that a CO desorption from the O-precovered Ru(0001) surface takes place between 300 K and 400 K, if the initial O coverage exceeds 2–3 ML [24]. The binding energy of CO on O-rich Ru(0001) is markedly higher than that on the (1×1)-O phase over Ru(0001).

It is obvious that the O-rich phases on Ru(0001) are extraordinarily active for CO oxidation. The origin of this high activity is, however, still illusive. It is not clear how the CO adsorption on the O-rich Ru(0001) surfaces takes place. One possible scenario may be that the presence of the additional subsurface O could alter the electronic structure of the (1×1)-O lattice, allowing CO adsorption.

This chapter is aimed at the study of the structural properties of the O-rich phases on Ru(0001) with O coverages above 2–3 ML. First, we used O₂ for the preparation of O-rich phases so that we can compare our results directly with Böttcher et al.'s reactivity measurements [23, 24]. The O-rich phases prepared by using NO₂ were also studied, and their structures will be compared with the O-rich phases prepared with O₂. It will be demonstrated that the structures of the O-rich phases depend critically on the oxygen source, NO₂ or O₂, and on the sample temperature for the preparation.

4.2 Preparation of O-rich phases on Ru(0001)

To dose an extraordinarily high amount of O₂, we used the gas shower system,

whose details are described in section 2.1. The amount of O₂ exposed to the sample was recorded by the background pressure in the chamber during dosing. In the following, the amount of O₂ will be given in quotation marks ‘’, when the sample was exposed to O₂ through the gas shower. With ‘30000 L’ of O₂ at a sample temperature of 600 K, the O-rich phase with an O coverage of 2–3 ML was prepared. With ‘60000 L’ of O₂ at a sample temperature of 800 K, the O coverage was 20 ML. The O coverage was determined by integrating the corresponding TD spectrum. As a reference, we used the TD spectrum of the (2×1)-O phase, assuming a coverage of 0.5 ML.

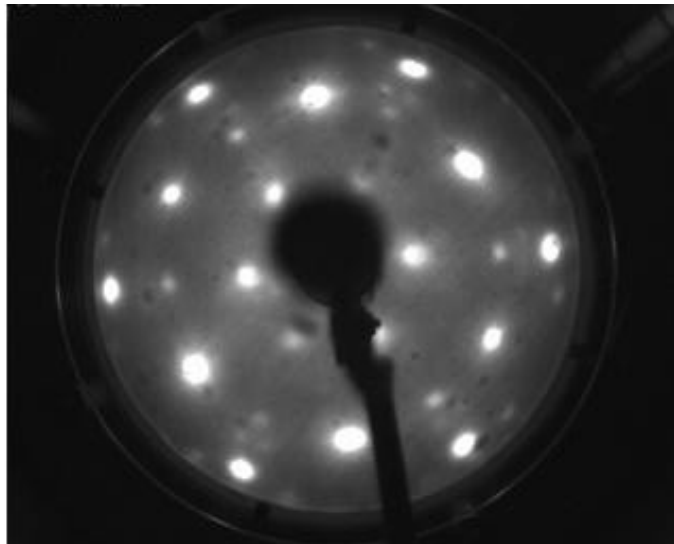
At sample temperatures between 800 K and 1050 K, one can prepare O-rich phases with O coverages of 30 ML or more. The O-rich phases prepared at the sample temperature of 1050 K disclose structural properties that are different from those of O-rich phases prepared at 600–800 K.

In addition, we studied the O-rich phases, which are produced by exposing NO₂. At a sample temperature of 600 K, 500 L of NO₂ was exposed by backfilling the chamber to prepare the O-rich phase with an O coverage of 5 ML.

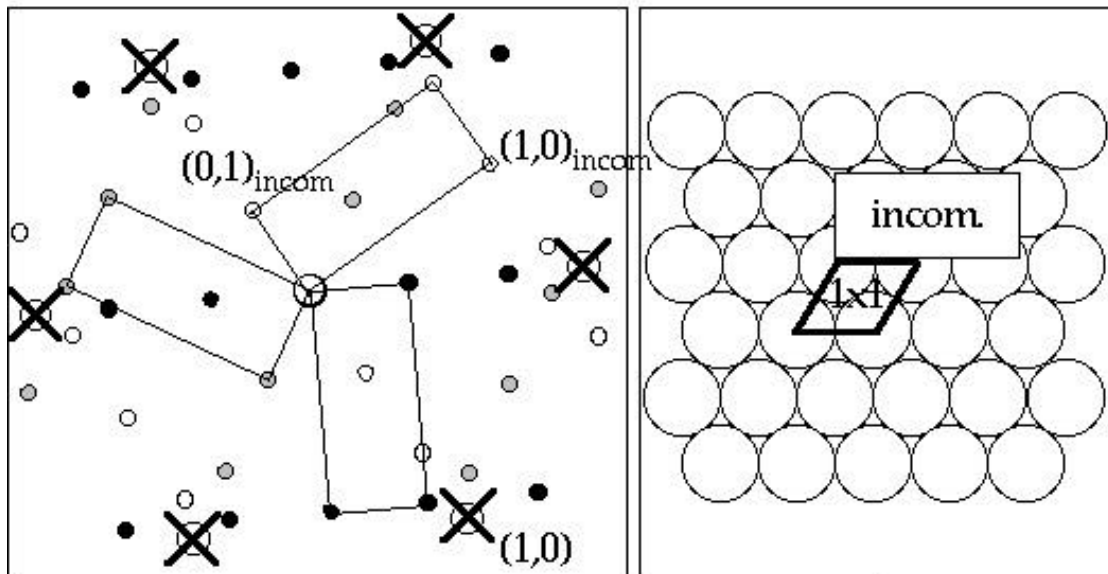
4.3 O-rich phases prepared by O₂ exposures at 600–800 K

The (1×1)-O is formed at an O coverage of 1.0 ML. At O coverages about 1–2 ML, only a (1×1) LEED pattern is observable, and the LEED I/E curves are identical to those of the (1×1)-O. The LEED pattern shows additional spots at O coverages above 2–3 ML. In Fig. 4.2 a), a typical LEED pattern is shown for the O-rich phases prepared by O₂ exposures at sample temperatures between 600 K and 800 K. The intensities of the additional spots increase with increasing O coverage, while the intensities of the integer-order beams decrease. The O coverage reaches 20 ML by exposing ‘60000 L’ of O₂ at 800 K. Here, the integer-order beams disappear, and only the superstructure beams remain visible.

This superstructure can be interpreted as a superposition of three different rotational



a)



b)

c)



 : integer-order beams
 : incommensurate overlayer

Fig. 4.2. a) LEED pattern of the O-rich phase over Ru(0001) prepared at 600 K by exposing '60000 L' of O₂ (g). The O coverage was 6 ML. The energy of the incident electron beam was 63 eV, and the sample temperature was 110 K. b) A schematic picture of the LEED pattern a) and its interpretation. The incommensurate LEED pattern can be explained by a superposition of three rotational domains with a rectangular unit cell. c) The unit cell of the incommensurate overlayer on Ru(0001) in the real space. The unit cell of the (1×1) structure is also drawn.

domains, whose unit cell is rectangular in shape (Fig. 4.2b)). This superstructure is incommensurate with respect to the substrate.

The incommensurate LEED pattern is frequently observed for the oxide formation. The incommensurate superstructure in Fig. 4.2a) may be an indication of the RuO_2 formation. It is known that RuO_2 is the only stable solid species formed by heating Ru metal in O [85], while the other Ru oxides such as RuO_3 and RuO_4 are volatile [85]. The structure of RuO_2 is illustrated in Fig. 4.3. The blue-black RuO_2 crystals are tetragonal with a rutile structure. The closest Ru–Ru distance is 3.11 Å. Ru–O bond lengths were estimated to be 1.91 Å and 2.01 Å. Each Ru makes two short Ru–O contacts and four long contacts. RuO_2 is a metallic oxide. The resistivity of RuO_2 is $3.5 \times 10^5 \Omega\text{cm}$ [86].

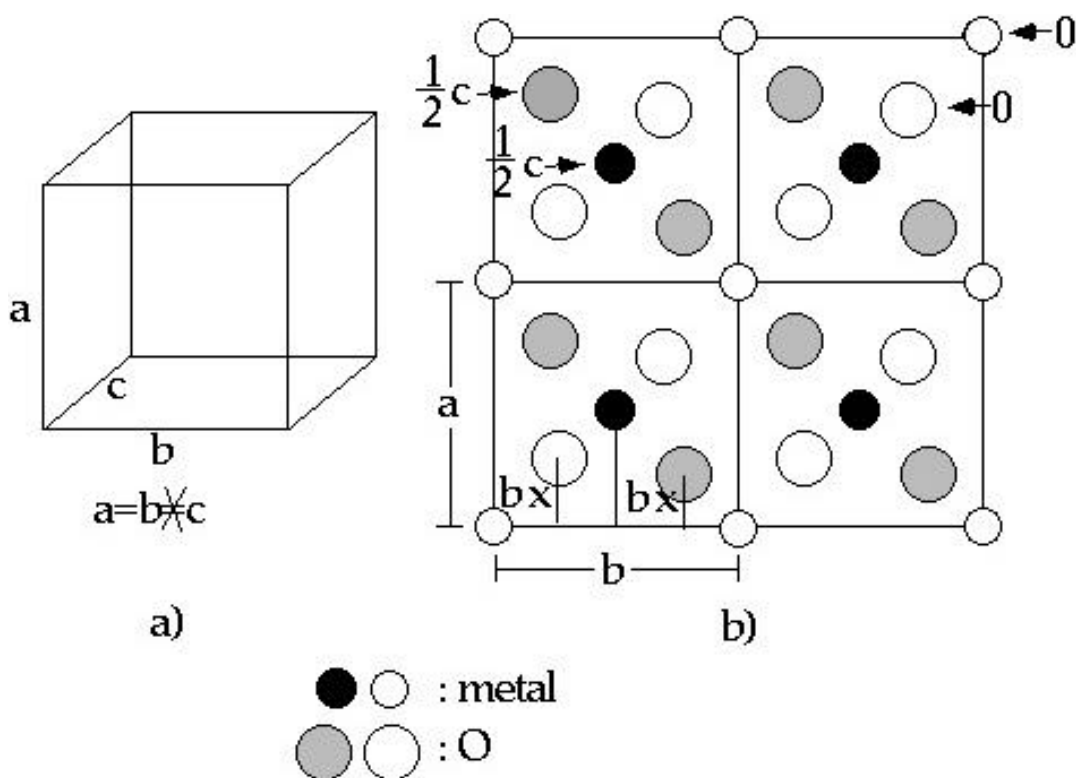


Fig. 4.3. a) The unit cells of the rutile structure. b) Atomic position of metal and O atoms in the rutile structure. The atomic coordinate for the c direction is given in the figure. In general, x is equivalent to 0.3 [87].

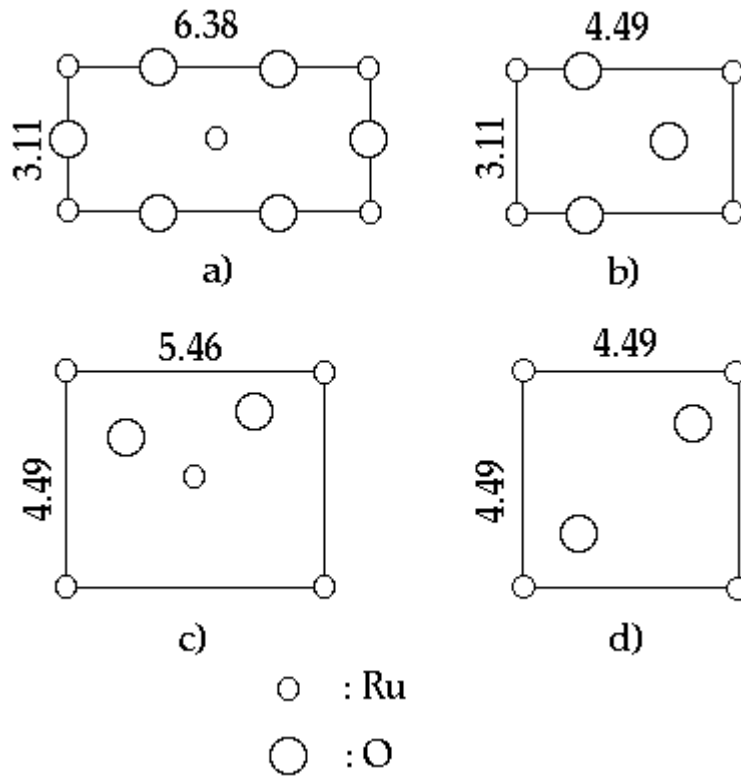


Fig. 4.4. Various low-index faces of RuO_2 : a) (110), b) (100), c) (101), d) (001). The values are given in \AA .

In Fig. 4.4, various low-index surface terminations of RuO_2 are illustrated. We compare the unit cell size of the incommensurate superstructure on the O-rich $\text{Ru}(0001)$ surface to those of the various terminations from bulk RuO_2 . The unit cell size of the incommensurate superstructure on the O-rich $\text{Ru}(0001)$ surface turns out to be $6.40 \pm 0.3 \text{ \AA} \times 3.10 \pm 0.2 \text{ \AA}$. The size of the unit cell of $\text{RuO}_2(110)$ is in agreement with that of the incommensurate superstructure of O-rich $\text{Ru}(0001)$. Consequently, $\text{RuO}_2(110)$ is exposed parallel to the $\text{Ru}(0001)$ surface at O coverages above 2–3 ML. This result is different from the previous investigations, where no oxide formation at these O coverages was observed, when NO_2 was used for the preparation [25, 44, 45].

In Fig. 4.5, the I/E curves of the integer-order beams from the LEED pattern in Fig. 4.2a) were compared with those of the clean $\text{Ru}(0001)$ surface and the pure

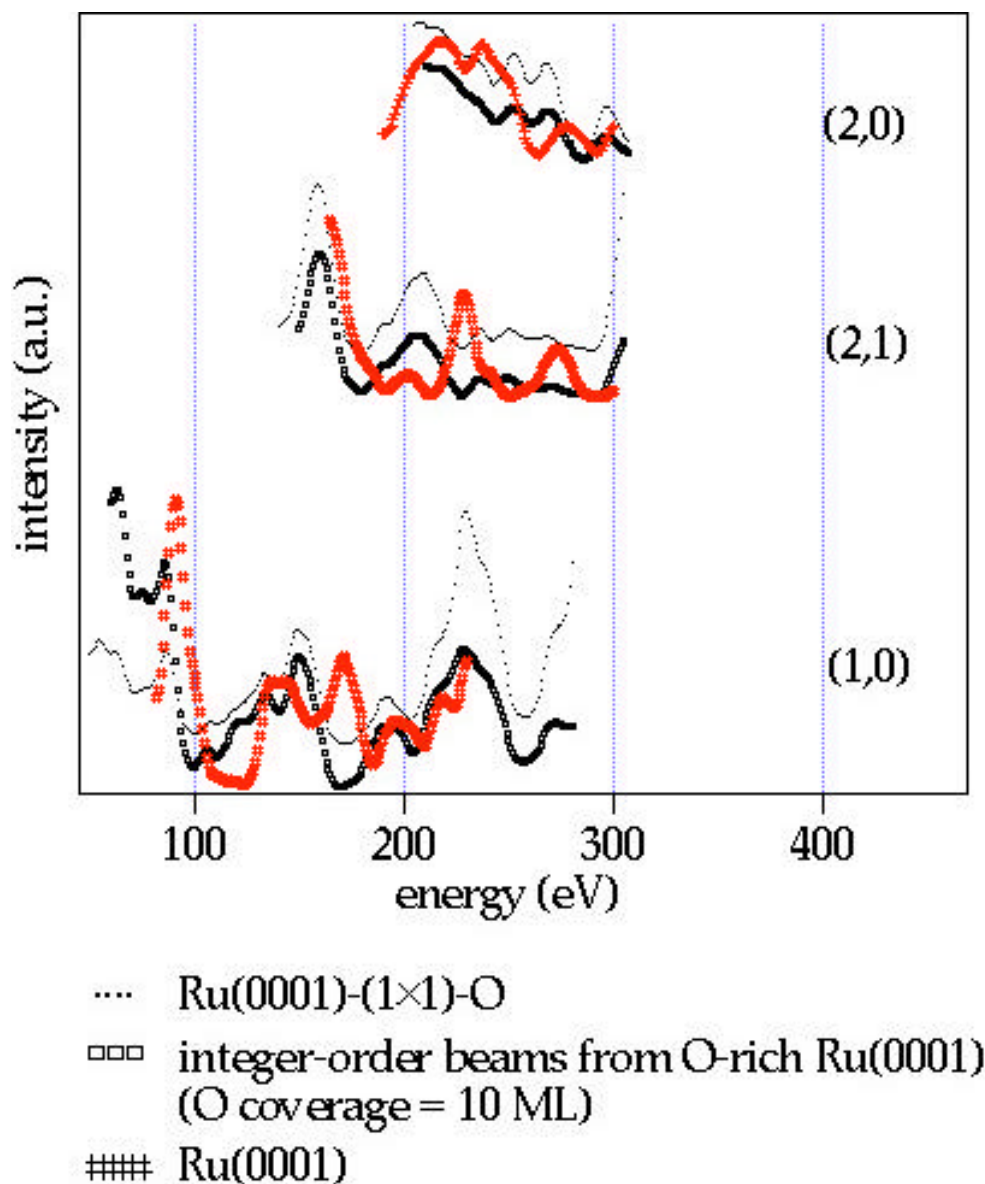


Fig. 4.5 The LEED I/E curves of the integer-order beams from a LEED pattern as Fig. 4.2a), the pure (1×1)-O phase on Ru(0001) and the clean Ru(0001) surface are compared. A striking similarity between the I/E curves from the (1×1)-O phase and those of the integer-order beams from the O-rich Ru(0001) surface can be observed ($R_p = 0.04$).

(1×1)-O overlayer on Ru(0001). The I/E curves of the bare Ru(0001) surface and those of the (1×1)-O are significantly different ($R_p = 0.83$) [26].

The comparison with the I/E curve of the (1×1)-O surface results in $R_p = 0.04$ (Fig. 4.3), which indicates that they are identical. Thus, the domains with a (1×1)

periodicity in the O-rich Ru(0001) surfaces consist of (1×1)-O patches.

4.4 CO adsorption on O-rich phases over Ru(0001)

To investigate the CO adsorption on the O-rich phases showing a LEED pattern as Fig. 4.2a), intensities of the integer order-beams and the superstructure beams were measured while dosing CO at a sample temperature of 100 K. The LEED I/E curves were collected before and after CO exposure (Fig. 4.6).

The intensity of the (1,0) beam does not vary during dosing CO, neither do LEED I/E curves of the integer-order beams. In contrast, the superstructure beams show a significant alteration during CO exposure. The intensities of $(0,1)_{\text{incom}}$, $(1,0)_{\text{incom}}$, and $(0,2)_{\text{incom}}$ decrease, and the intensity of $(1,1)_{\text{incom}}$ increases. The I/E curves of the superstructure beams change significantly after dosing CO.

The intensity change of the LEED beams during dosing CO indicates CO adsorption on O-rich phases of Ru(0001) on a well-defined adsorption site. In addition, this observation enables us to discriminate among the different possibilities for the morphology of the O-rich Ru(0001) surface, which will be described in the following.

Model A: After completion of the (1×1)-O phase, further O adsorption results in the formation of the oxide layer overgrowing the (1×1)-O overlayer (Fig. 4.7). For model A, the expected variation of the LEED beam intensities upon CO adsorption is the following.

CO molecules can adsorb selectively on specific adsorption sites, or they can form a disordered phase. Occupation of specific adsorption sites causes changes of the I/E curves of the oxide layers. In a beam intensity measurement as a function of CO doses, the intensities of the beams from the oxide layers will change. The shape of the I/E curves for the (1×1)-O phase will not alter upon CO adsorption, because the CO overlayer has no relationship with the periodicity of the (1×1)-O phase.

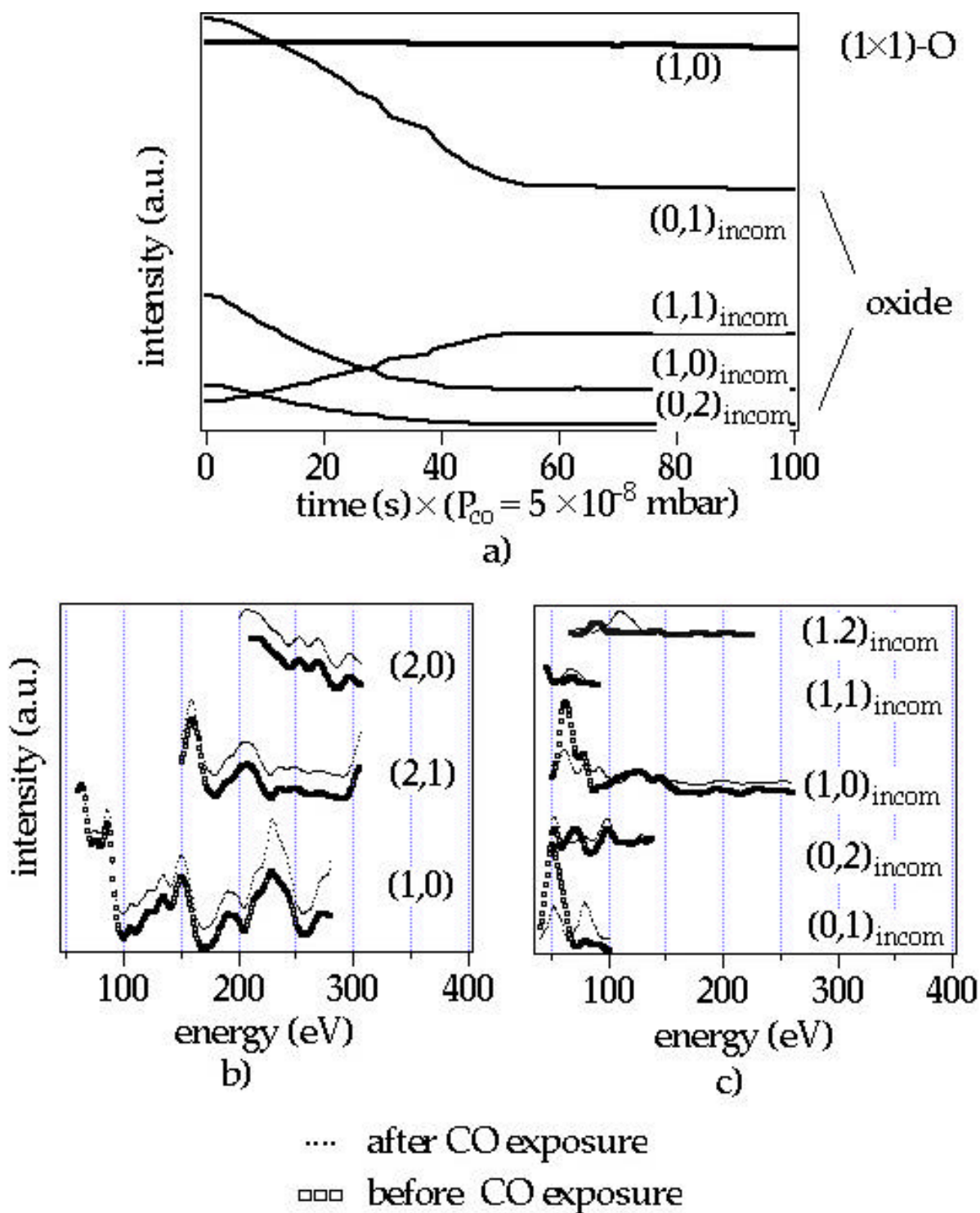


Fig. 4.6. a) Variation of LEED beam intensities during dosing CO on the O-rich Ru(0001) surface. b) The I/E curves of the integer-order beams before and after dosing CO. c) The I/E curves of the oxide structure before and after dosing CO.

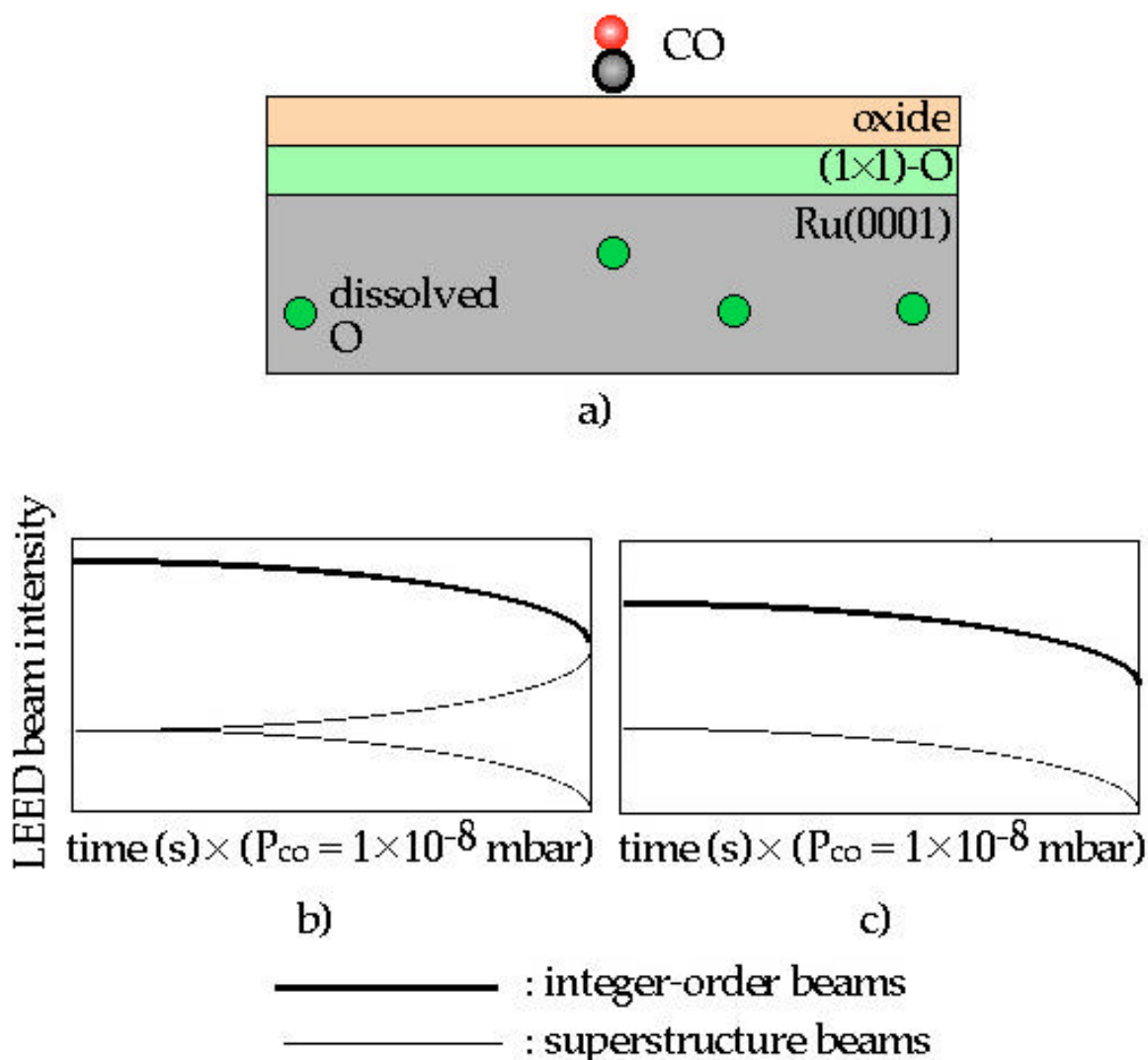


Fig. 4.7. a). CO adsorption on the model A surface. See text for details. b) Expected change of LEED beam intensities, if CO molecules adsorb on the model A surface with specific local geometries. c) Expected change of the LEED beam intensities, if CO forms a disordered overlayer on the model A surface.

However, their absolute intensities have to decrease. CO adsorption without any specific adsorption geometry will lead to a damping of all the LEED beams. These expectations contrast with our experimental observation so that model A can be ruled out.

Model B: After completion of the (1x1)-O overlayer, further O adsorption leads

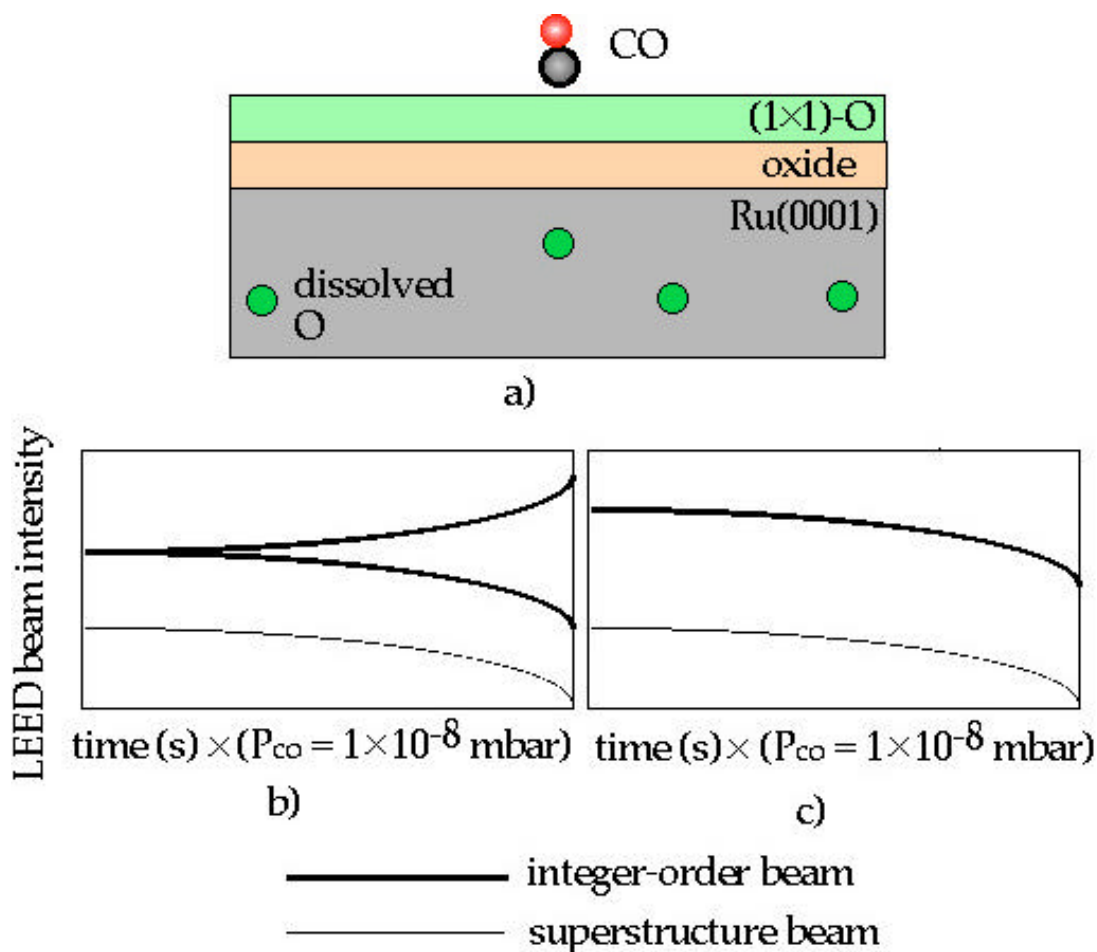


Fig. 4.8. a) CO adsorption on the model B surface. See text for details. b) Expected changes of the LEED beam intensities, if CO molecules adsorb on the model B surface with specific local geometries. c) Expected changes of the LEED beam intensities, if CO forms a disordered overlayer on the model B surface.

to the formation of an oxide structure below the (1×1)-O lattice (Fig. 4.8).

Two different ways of CO adsorption are possible: with or without specific geometries of CO molecules. In the former case, the I/E curves of the (1×1)-O phase will be changed upon CO adsorption. Intensities of the LEED beams related to the oxide layer should decrease without change of the shape of the I/E curves (Fig. 4.8b)). In the latter case, a decrease of the intensities of all the beams is expected, while the shape of the I/E curves does not change (Fig. 4.8c)). These changes are not reconciled in our experiment.

Model C: Separate oxide islands are formed beside the (1×1)-O phase, and CO adsorption takes place (Fig. 4.9).

If CO molecules adsorb only on the (1×1)-O domains, the I/E curves of the (1×1)-O related LEED beams change either in shape or in absolute intensity. The beams from the oxide islands will not undergo any change (Fig. 4.9b)).

If CO molecules adsorb selectively on the oxide islands, the I/E curves of the oxide islands will be changed after CO exposure. The intensities of the LEED beams from the oxide islands will be changed during dosing CO. In this case, the (1×1)-O beams are not affected by CO adsorption (Fig. 4.7c)). This is observed in our experimental results.

We can conclude that the O-rich phases consist of the (1×1)-O domains and separate oxide islands. CO adsorbs only on the oxide islands. This was later also confirmed by STM investigations [88]. They found the coexistence of large oxide islands and (1×1)-O domains for O-rich phases of Ru(0001). From the STM investigations, the thickness of the oxide islands was estimated to be 10–20 Å. This is in accordance with the X-ray reflection measurements, in which the thickness of 20 ± 10 Å was determined [89]. The adsorption of CO molecules on the oxide islands was also confirmed in these STM investigations.

The results of thermal desorption experiments from the CO covered O-rich Ru(0001) surfaces are shown in Fig. 4.10. CO desorbs between 230 K and 600 K, which is accompanied by the CO₂ desorption between 200 K and 350 K. The desorption temperature of CO from the O-rich phases over Ru(0001) is much higher than that of other oxides, such as TiO₂ [90], NiO [91, 92] and MgO [93, 94]. On these surfaces, CO desorption completes below 200 K.

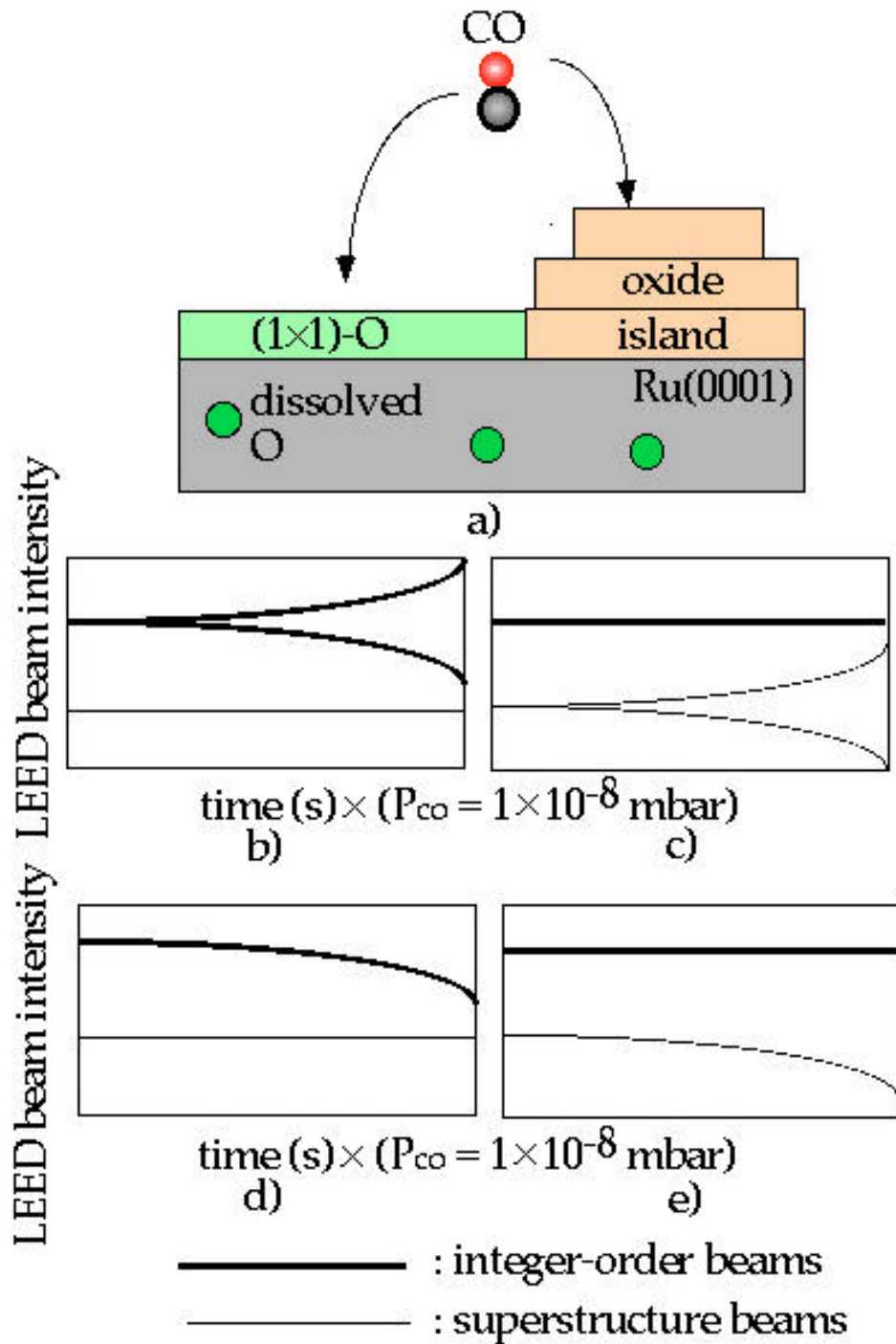


Fig. 4.9. a) CO adsorption on the model C surface. See text for details. b) Expected changes of the LEED beam intensities, if CO molecules adsorb only on the (1×1)-O domains with specific adsorption geometries. c) Expected changes of the LEED beam intensities, if CO molecules adsorb only on the oxide islands with specific adsorption geometries. d) Expected changes of the LEED beam intensities, if CO molecules adsorb only on the (1×1)-O domain and form a disordered structure. e) Expected changes of the LEED beam intensities, if CO molecules adsorb only on the oxide islands and form a disordered structure.

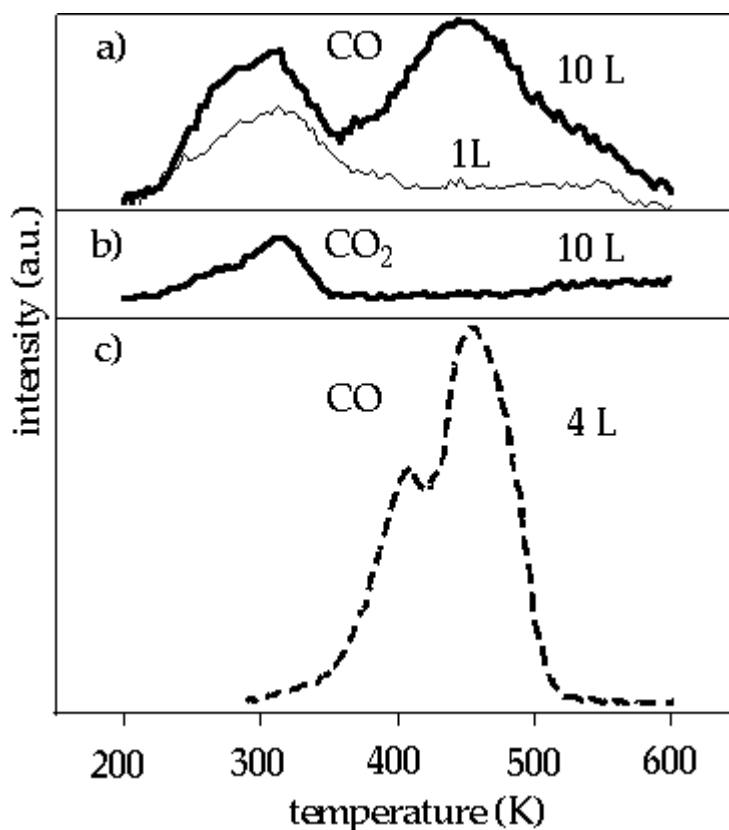


Fig. 4.10. TD spectra of a) CO and b) CO₂ after exposing the O-rich Ru(0001) surface with an O coverage of 10 ML to CO at 100 K. c) TD spectrum of CO from the bare Ru(0001) surface. The amounts of CO doses are also given. The heating rate was 3 K/s.

4.5 Structure analysis of the oxide islands by LEED I/E analysis

We estimated the size of the unit cell for the incommensurate superstructure in Fig. 4.2a) to be similar to that of RuO₂(110). Therefore, we concluded that RuO₂(110) is exposed on the O-rich Ru(0001) surface. RuO₂(110) is not growing above or below the (1×1)-O, but separate RuO₂(110) islands are formed. In this section, we discuss the atomic surface structure of the RuO₂(110) islands.

There are several possible structure models for the RuO₂(110) surface (Fig. 4.11).

The first model is a termination with on-top O atoms (Fig. 4.11A). On this surface,

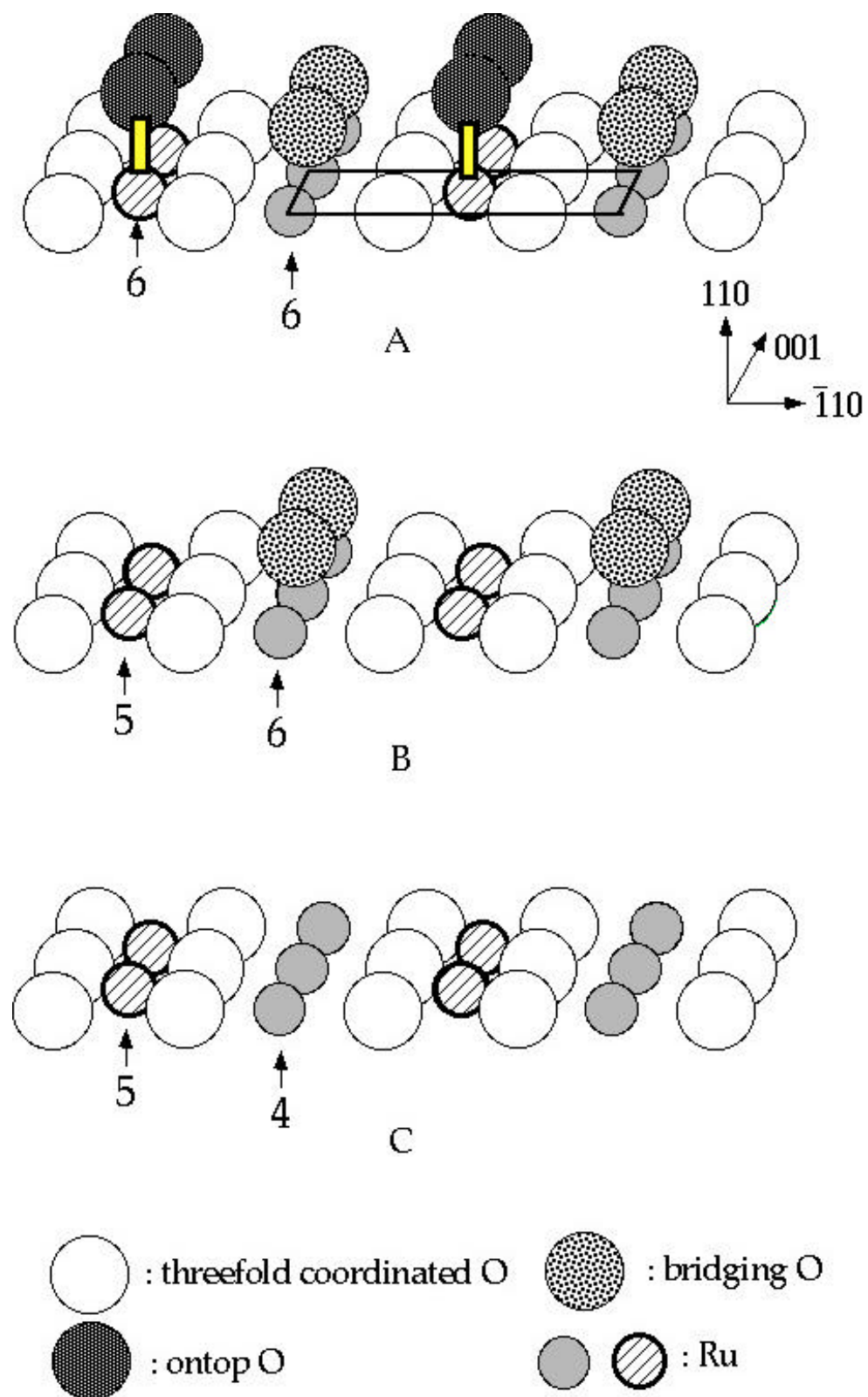


Fig. 4.11. Possible structure models for the $\text{RuO}_2(110)$ surface are depicted. A: on-top O termination. B: bridging O termination. C: (Ru + threefold coordinated O) termination. The coordination numbers of Ru atoms are also shown.

three different O atoms are exposed. One O atom is located directly above the Ru atom (on-top), the second forms a bridge bond with two underlying Ru atoms and the third is threefold coordinated to Ru atoms (bulk-like).

A second possible model is a RuO₂(110) surface, which is terminated by bridging O atoms (Fig. 4.11B). The structure investigation of TiO₂(110) revealed that the TiO₂(110) surface exposes bridging O arrays as depicted in Fig. 4.11B [95].

The RuO₂(110) surface may not contain either the on-top or the bridging O (Fig. 4.11C). The Ru and the threefold coordinated O atoms are in the topmost surface plane.

The surface structure of the oxide islands was determined on atomic scale by employing quantitative LEED I/E analysis. After exposing the bare Ru(0001) surface to '60000 L' of O₂ at 600 K, the RuO₂(110) related I/E curves from eight non-equivalent beams were collected with the total energy range of 850 eV. The vertical positions of following atoms were refined in I/E calculations: on-top O, bridging O, atoms in first (threefold O+Ru) plane, first O bilayer, second (threefold O+Ru) plane, and second O bilayer. The lateral position of the threefold coordinated O atoms in the first plane was also varied along ($\bar{1}10$) direction during the fit procedure. Ru and O atoms in deeper layers were kept at bulk positions. The Debye temperatures of the on-top and bridging O atoms, the Ru and O atoms in the first main plane and the O atoms in the first O bilayer were refined. The Debye temperatures of O and Ru in deeper layers were fixed to 600 K and 420 K, respectively.

From the quantitative LEED I/E analysis, a clear preference for the termination with bridging O atoms (model B) is inferred. The best R_p achieved were 0.61 for Model A, 0.36 for Model B, and 0.51 for Model C.

Next, we varied the occupation factors of the bridging O, threefold coordinated O atoms in the first Ru+O plane and the O atoms in the first O bilayer in model B, and carried out the I/E calculations again. The main objective of these calculations is to determine the density of the O defects at the surface. Oxygen defects on TiO₂

and NiO play an important role for the catalytic activity of these surfaces. For instance, the binding energies of CO on defects of TiO₂ and NiO were significantly increased. [90–92]. Equally, defect sites on RuO₂(110) may be responsible for the high catalytic activity, while the perfect RuO₂ surface is not active for the catalytic CO oxidation.

However, the calculations gave a best agreement between theory and experiment, when the O occupation factors were 100 %. Consequently, the oxide islands expose a perfect RuO₂ surface with a negligible amount of O defects. This conclusion is in line with STM investigations, where defective RuO₂(110) patches on Ru(0001) were not observed [88].

In Fig. 4.12, the best-fit structure of the RuO₂(110)/Ru(0001) determined by LEED I/E analysis is reproduced. In addition, the experimentally determined parameters are compared with those derived from DFT calculations by A.P. Seitsonen [96]. The agreement between the results of DFT calculations and those of LEED I/E calculations is excellent. The LEED I/E curves calculated for the best-fit geometry and the experimental I/E curves are compared in Fig. 4.13.

As shown in LEED and DFT, the as-grown RuO₂(110) domains expose complete arrays of the bridging O atoms. The O atoms in the bulk RuO₂ are threefold coordinated. In a concept of atomic orbital hybridization, the valence orbitals of the threefold coordinated O atoms are hybridized to sp² hybrid orbitals. On the other hand, Ru atoms in the bulk RuO₂ are sixfold coordinated, and the valence orbitals of Ru atoms are hybridized to d²sp³ hybrid orbitals. Assuming that the valence orbitals of the bridging O and the fivefold coordinated Ru atoms (this Ru atom is referred to as cus atom, where cus is the abbreviation for ‘coordinatively unsaturated site’ [88]) hybridize in similar ways as the Ru and O atoms in the bulk RuO₂, the bridging O and fivefold coordinated or cus Ru atoms create dangling bonds, because they are undercoordinated. The bridging O and cus Ru produce one dangling bond, respectively, creating two dangling bonds per unit cell on the model B surface. In models A and C, in contrast, three dangling bonds per unit cell are present.

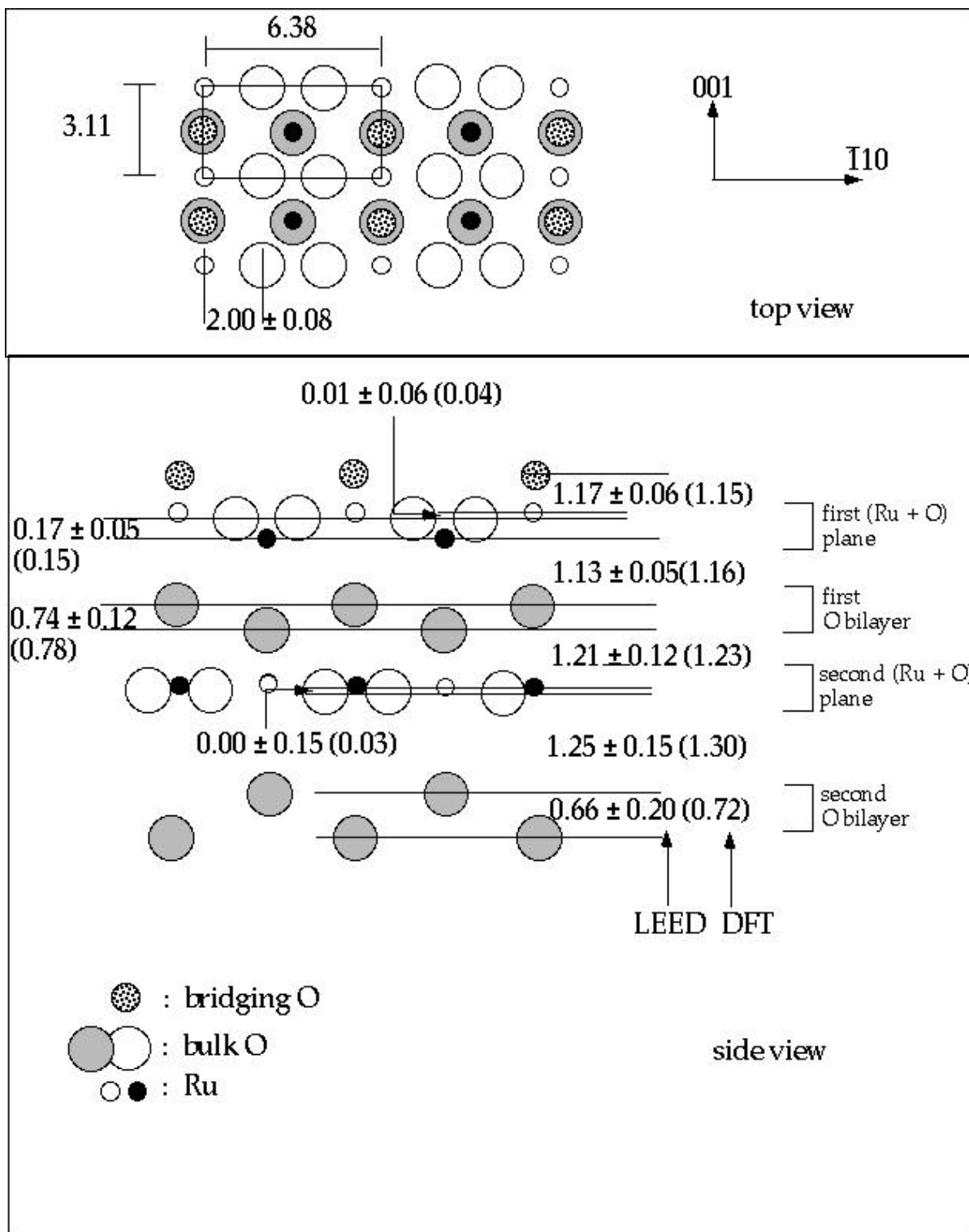


Fig. 4.12. Best-fit structure of RuO₂(110) on Ru(0001) determined by the LEED I/E analysis and DFT calculations [96]. The values are given in Å.

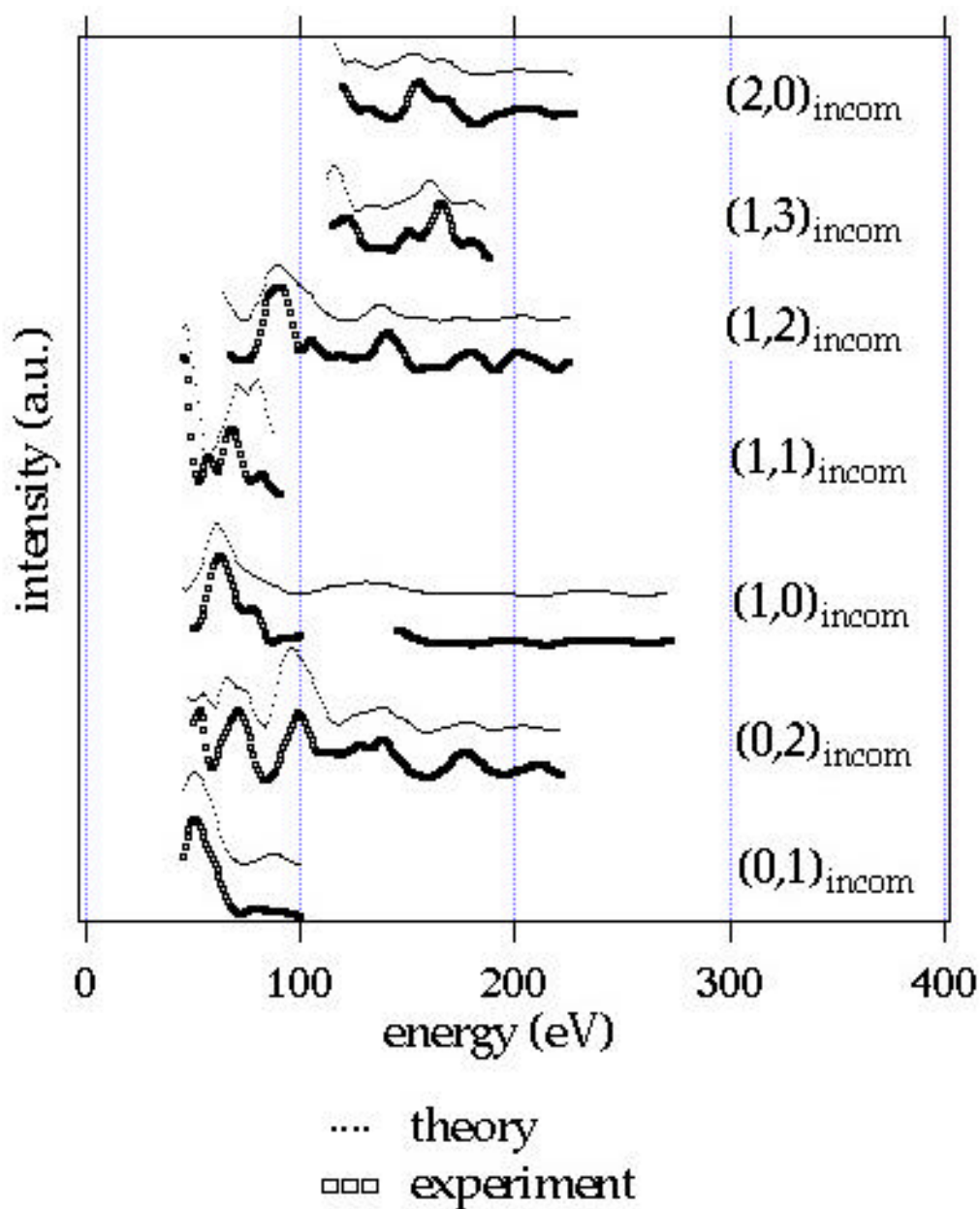


Fig. 4.13. The experimental LEED I/E curves are compared with calculated ones for the best-fit structure of $\text{RuO}_2(110)/\text{Ru}(0001)$ ($R_P = 0.36$).

The on-top O in Model A and the fourfold coordinated Ru in model C create two dangling bonds, respectively. The $\text{RuO}_2(110)$ surface termination by bridging O arrays is reasonable, as it creates a minimum number of dangling bonds.

The bridging O atoms are 1.17 Å above the Ru cations, giving rise to a Ru–O bond length of 1.95 Å. The bond length between the bridging O and Ru (1.95 Å) is shorter than the bulk value (2.01 Å) by 3 %. This result is quite different from that of TiO₂(110) [95]. The bridging O atoms of TiO₂(110) are displaced inwardly by 0.3 Å with respect to the bulk position. This causes the Ti–O_{br} bond length to be shorter than the bulk value by 10 %. This experimental observation is, however, not consistent with theoretical studies [97–99]. Such a large relaxation could not be found in theoretical studies. To examine the reasons for this poor agreement between theoretical calculations and experiments, all-electron first principle calculations were conducted [100]. A very soft, anisotropic and anharmonic surface rigid-unit vibrational mode was found, which involves displacements of the surface ions of approximately 0.15 Å for thermal vibrations corresponding to room temperature. Quite in contrast, for RuO₂(110), DFT and LEED calculations give identical structures. The optimum Debye temperature of the bridging O is 500 K, which is comparable to that of the threefold O atom (600 K). Thus, the soft vibrations of the bridging O atoms on RuO₂ (110) are ruled out.

To illustrate the sensitivity of our LEED I/E analysis to the layer distance between the bridging O and the attached Ru atoms, $d(\text{Ru}-\text{O}_{\text{br}})$, we varied this parameter in steps of 0.05 Å in a wide range of parameter space from 0.6 Å to 1.4 Å and plotted optimum R_{p} in Fig. 4.14. Apparently, there are two local minima in R_{p} , one at 0.6 Å and the other at 1.2 Å. The value of 0.6 Å can be excluded, as it leads to unreasonably small Ru–O lengths. Recently, a photoelectron diffraction study of RuO₂(110) was published [101]. Essentially, the structural parameters agree favorably with the results of the present work except for the layer distance between the bridging O and the attached Ru atoms, which is 0.2 Å shorter (1.0 Å) than our value. The optimum R_{p} of the model B keeping the $d(\text{Ru}-\text{O}_{\text{br}})$ at 1.0 Å is, however, 0.7 (Fig. 4.14). This value is markedly higher than for $d(\text{Ru}-\text{O}_{\text{br}}) = 1.2$ Å so that the XPD derived value can be safely excluded.

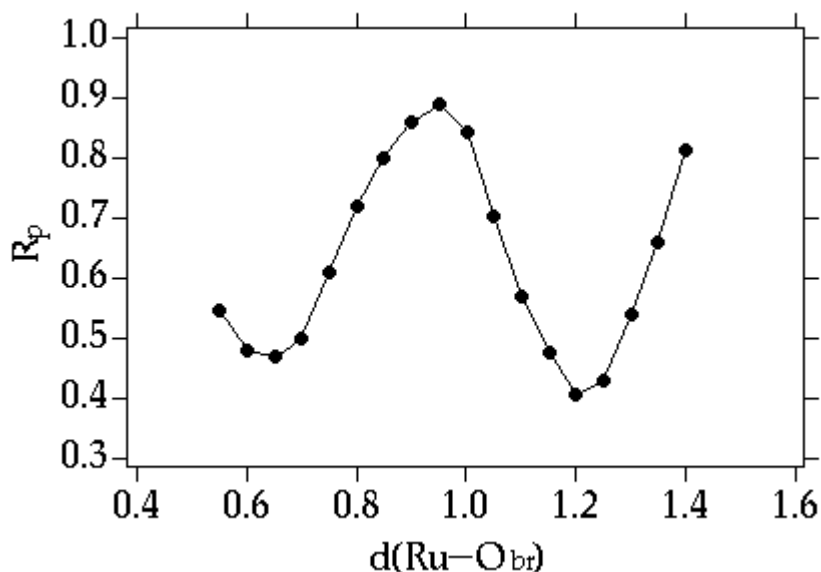


Fig. 4.14. R_p as a function of the layer distance between the bridging O and the attached Ru atoms, $d(\text{Ru}-\text{O}_{\text{br}})$.

4.6 Determination of the adsorption geometry for CO on $\text{RuO}_2(110)/\text{Ru}(0001)$

After exposing the $\text{RuO}_2(110)/\text{Ru}(0001)$ surface to 100 L of CO at 100 K, the LEED I/E curves of eight symmetrically inequivalent beams were collected with the total energy range of 890 eV. The I/E curves of $\text{RuO}_2(110)/\text{Ru}(0001)$ change significantly upon CO exposure (Fig. 4.6). R_p between the I/E curves from the $\text{RuO}_2(110)/\text{Ru}(0001)$ surface collected before and after exposing 100 L of CO at 100 K is 0.54. Obviously, CO adsorption on $\text{RuO}_2(110)/\text{Ru}(0001)$ takes place, and CO molecules occupy specific adsorption sites.

Four different adsorption sites can be proposed for CO on $\text{RuO}_2(110)/\text{Ru}(0001)$, the on-top (Fig. 4.15 A), the bridge site (Fig. 4.15), positioning above two bridging O atoms and forming carbonate species (Fig. 4.15C), and on top of the bridging O (Fig. 4.15 D). In model B, CO can be attached to two cus Ru atoms, or CO makes a bridge configuration with two underlying

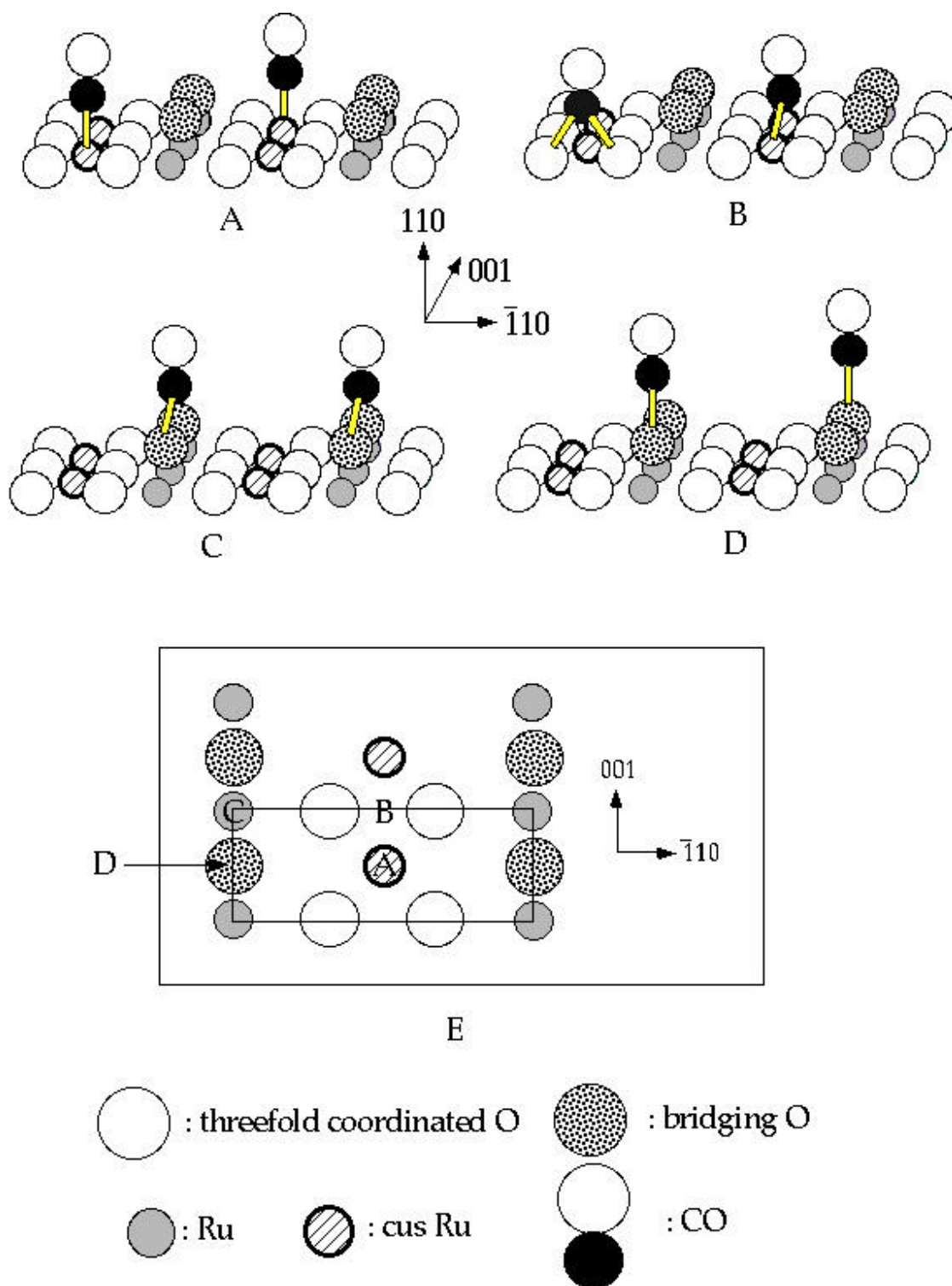


Fig. 4.15. Possible adsorption sites of CO on RuO₂(110)/Ru(0001) A: On-top site. B: Forming carbonate complex with two threefold O atoms or bridge bonding with two cus Ru atoms (bridge site). C: Forming carbonate complex with two bridging O atoms. D: On top of bridging O. E: Top view of RuO₂(110)/Ru(0001) is reproduced in the inset. The adsorption sites (A, B, C and D) are also denoted.

threefold coordinated O atoms (carbonate species). It is not clear which configuration from these two possibilities would be preferred, if CO molecules sat on the bridge sites. Leaving this question open, the four models were tested for CO on RuO₂(110)/Ru(0001) in the LEED I/E analysis. The Debye temperatures and atomic positions of C and O atoms of the CO molecule, bridging O, Ru and threefold O in the first main plane and O atoms in the first O bilayer were released in the fit procedure. The atoms in deeper layers were kept at the same positions as in the best-fit structure of RuO₂(110)/Ru(0001) (Fig. 4.12).

First, we did not include any CO on RuO₂(110)/Ru(0001) in the I/E calculations. These calculations gave an optimum R_p of 0.78, showing a bad agreement between theory and experiment.

From the four possibilities (Fig. 4.15 A, B, C and D), the on-top site (Fig. 4.15A) gave a much better agreement between experiment and theory (R_p = 0.30) than the bridge site (Fig. 4.15B, R_p = 0.51), above two bridging O (Fig. 4.15C, R_p = 0.70) and on top of bridging O (Fig. 4.15D, R_p = 0.63). The experimental I/E curves and the calculated ones for the best-fit structure are compared in Fig. 4.16.

In Fig. 4.17, the best-fit structure of CO on RuO₂(110)/Ru(0001) is illustrated. Here again, for comparison, the results of DFT calculations [102] are presented. The agreement between the experimentally found structural parameters and the results of DFT calculations is excellent. The bond length of C–O and Ru–C are 1.12 Å and 2.00 Å, respectively, and they are comparable to those of the ($\sqrt{3}\times\sqrt{3}$)R30°-CO on Ru(0001), in which the Ru–C and C–O distances are 1.93 Å and 1.10 Å, respectively [78].

From DFT calculations, the binding energy of CO on RuO₂(110)/Ru(0001) is 1.2 eV, but 1.8 eV on Ru(0001) [88]. Thus, CO on RuO₂(110)/Ru(0001) is less stable than on the bare Ru(0001) surface. However, a binding energy of 1.2 eV is much higher than the binding energies of CO on the other oxides. On common oxides, typical CO binding energies are below 0.7 eV [103]. The relatively high binding energy of CO on RuO₂(110)/Ru(0001) was already identified in thermal desorption

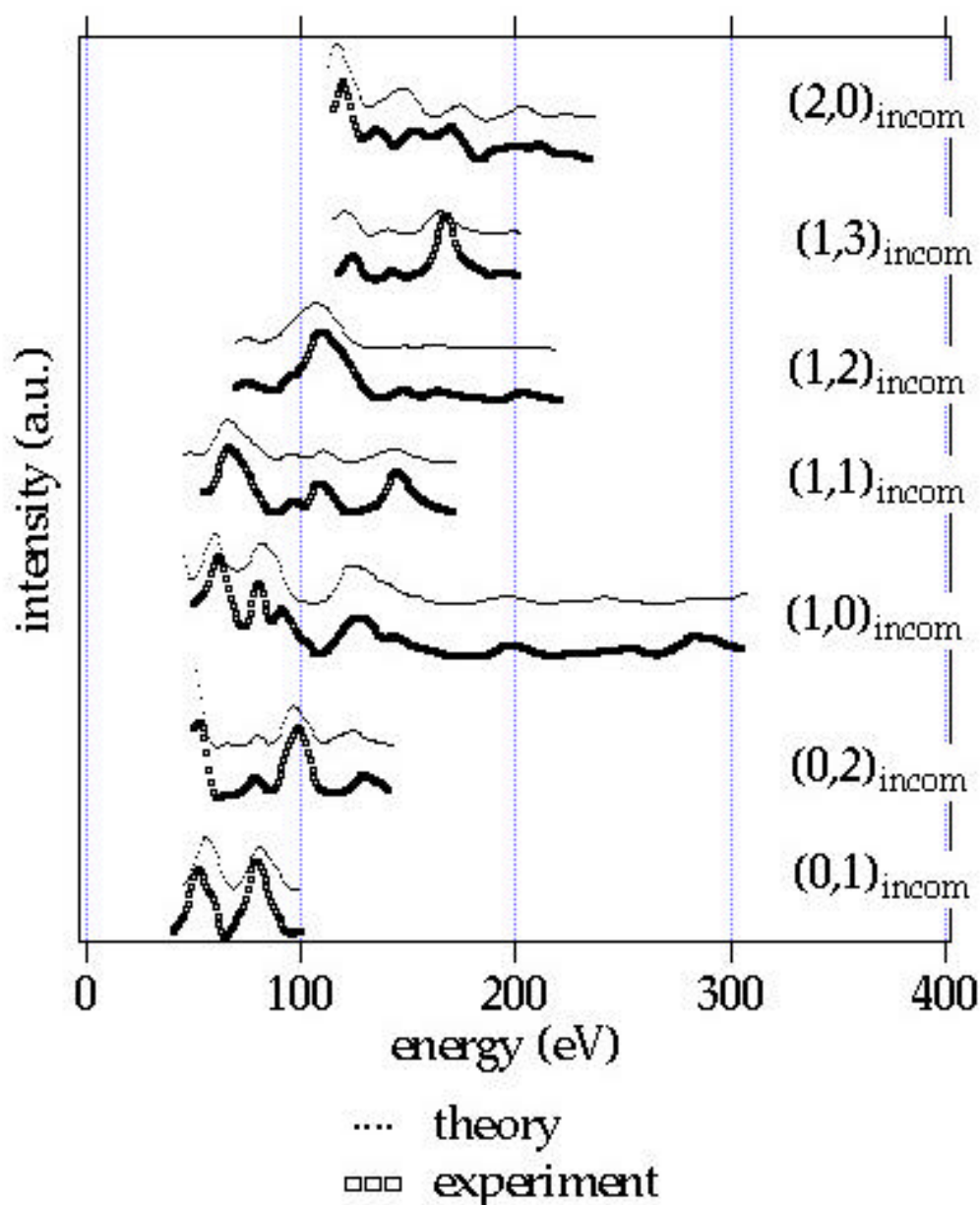


Fig.4.16. The experimental LEED I/E curves are compared with the calculated ones for the best-fit structure of CO on RuO₂(110)/Ru(0001). ($R_p = 0.30$)

experiments (Fig. 4.10). The strong bonding of CO on RuO₂(110) can be rationalized by the presence of d electrons of RuO₂ at the Fermi level [104, 105], which is a typical characteristic for metals. The d electrons at the Fermi level can facilitate π backdonation. Quite in contrast, common oxides contain no d electrons at the Fermi level, resulting in low adsorption energies of CO.

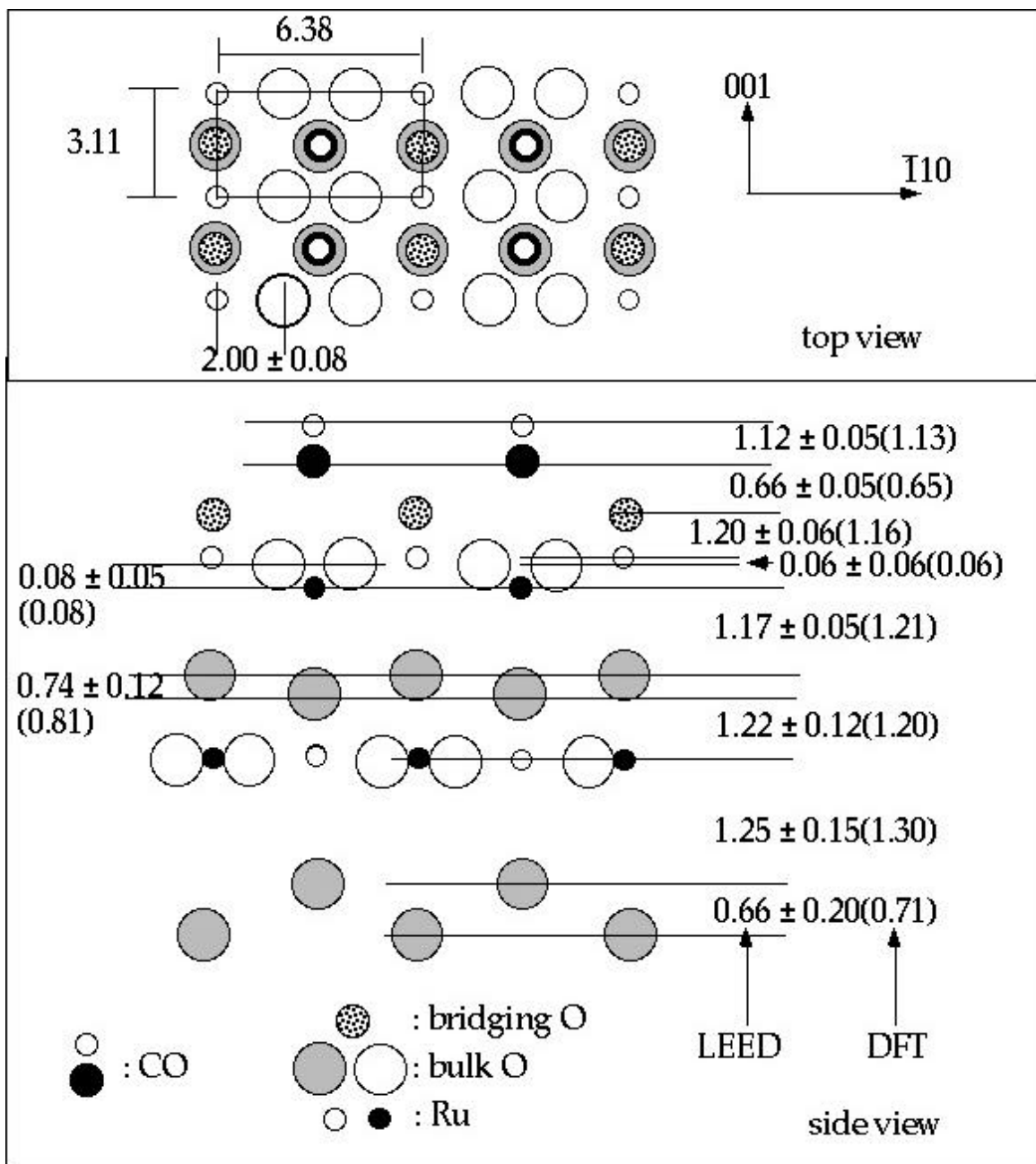


Fig. 4.17. Best-fit structure of CO on RuO₂(110)/Ru(0001) determined by I/E calculations and DFT calculations. The values are given in Å.

In the Langmuir-Hinshelwood mechanism, high binding energies of CO and low binding energies of atomic O are important factors for the catalytic activity of the CO oxidation. According to DFT calculations, the binding energy of bridging O of RuO₂(110)/Ru(0001) is 1.6 eV, which is even lower than that of O atoms in the

Ru(0001)-(1×1)-O phase [88]. Due to the relatively high binding energy of CO and the low binding energy of O on RuO₂(110)/Ru(0001), one can expect that RuO₂(110) islands catalyze CO oxidation very efficiently. In fact, the RuO₂(110) related LEED beams disappeared after the O-rich Ru(0001) surface had been exposed to 100L of CO at a sample temperature of 500K. Recent STM investigations [88] revealed that a brief heating of CO covered RuO₂(110) layers to 500 K creates holes and Ru clusters on the originally defect-free surface. These LEED and STM results indicate that CO readily recombines with a lattice O atom of RuO₂(110) to CO₂. Therefore, we can conclude that RuO₂(110) formation is responsible for the high catalytic activity of O-rich Ru(0001) surfaces towards CO oxidation.

4.7 N₂ adsorption on RuO₂(110)/Ru(0001)

N₂ molecules, which are isoelectronic molecules to CO, adsorb on the Ru(0001) surface in a similar way as CO, i.e., adsorb vertically by attaching one N atom to the Ru surface, but with a substantially lower adsorption energy in comparison with CO [106, 107]. The N₂ adsorption energy on Ru(0001) increases with preadsorbed O atoms, while K (potassium) weakens Ru–N₂ bonding. The presence of O atoms can increase the sticking coefficient of N₂, while K suppresses N₂ adsorption. This suppression effect of K cannot be attributed to the site blocking, because CO readily adsorbs under similar conditions. The work function decreases upon N₂ adsorption [107], indicating formation of a Ru(-)–N₂(+) dipole layer. Apparently, the bonding mechanism of N₂ on Ru(0001) is mediated by *s* donation [107].

The binding energy of CO on RuO₂(110)/Ru(0001) (1.2 eV) is less than that on the clean Ru(0001) surface (1.8 eV). Taking into account the electron withdrawing nature of CO through the π backdonation, the cus Ru atoms on RuO₂(110)/Ru(0001) should be more acidic than the Ru atoms in the first layer of the bare Ru(0001) surface (acidic: electron accepting, basic: electron donating [1]). Thus,

the adsorption energy of N_2 on $RuO_2(110)$ islands over $Ru(0001)$ may be higher than that on the bare $Ru(0001)$ surface, if N_2 adsorbs vertically on top of cus Ru like CO.

First, in order to investigate the N_2 adsorption on the (1×1) -O overlayer, the I/E curves of the (1×1) -O phase before and after dosing 30 L of N_2 at 100 K were collected (Fig. 4.18). The (1×1) -O surface was prepared by exposing '30000 L' of O_2 at a sample temperature of 500 K. Obviously, no change of the LEED I/E curves

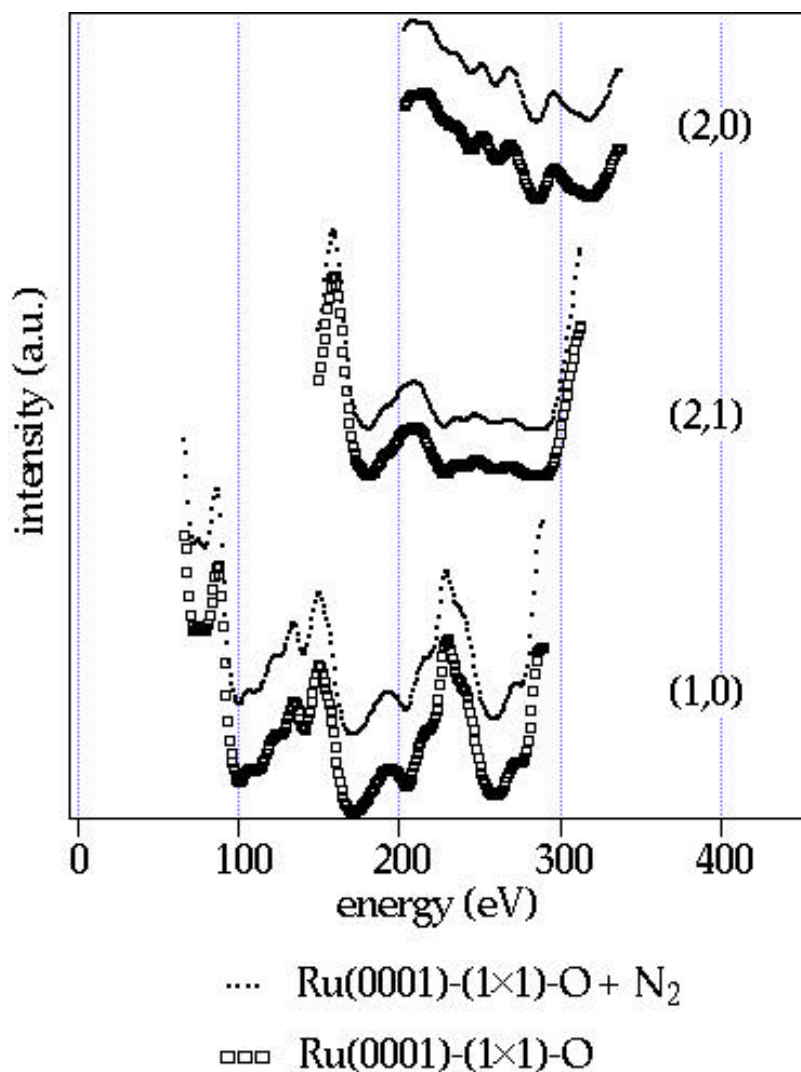


Fig. 4.18. The LEED I/E curves from the (1×1) -O phase before and after N_2 exposure at 100 K are compared ($R_p = 0.02$).

occurs after N_2 exposure, indicating that N_2 does not adsorb on the (1×1) -O phase at 100 K.

To study the adsorption of N_2 on the O-rich Ru(0001) surface with a LEED pattern like Fig. 4.2a), intensities of the (1×1) -O and $RuO_2(110)$ related LEED beams were measured during N_2 exposure at 100 K (Fig. 4.19). The (1×1) -O beams do not alter during N_2 exposure, while intensities of the $RuO_2(110)$ beams change significantly. From this result we can conclude that N_2 adsorbs selectively on the $RuO_2(110)$ islands.

After exposing $RuO_2(110)/Ru(0001)$ to 30 L of N_2 at 110 K, the I/E curves were collected from seven symmetrically non-equivalent beams with a total energy range of 960 eV. As is illustrated in Fig. 4. 20, the I/E curves from $N_2/RuO_2(110)/Ru(0001)$ are completely different from those of bare $RuO_2(110)/Ru(0001)$, indicating a well-

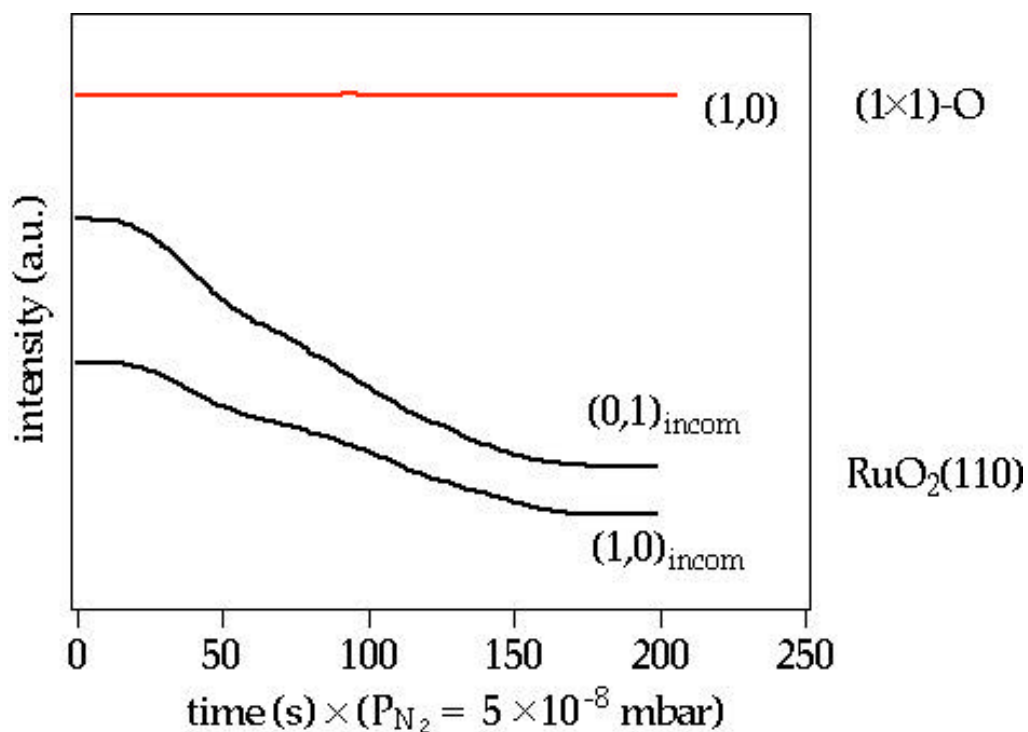


Fig. 4.19. Changes of the intensities of $RuO_2(110)$ and (1×1) -O related beams during N_2 exposure on the O-rich Ru(0001) surface at 100 K.

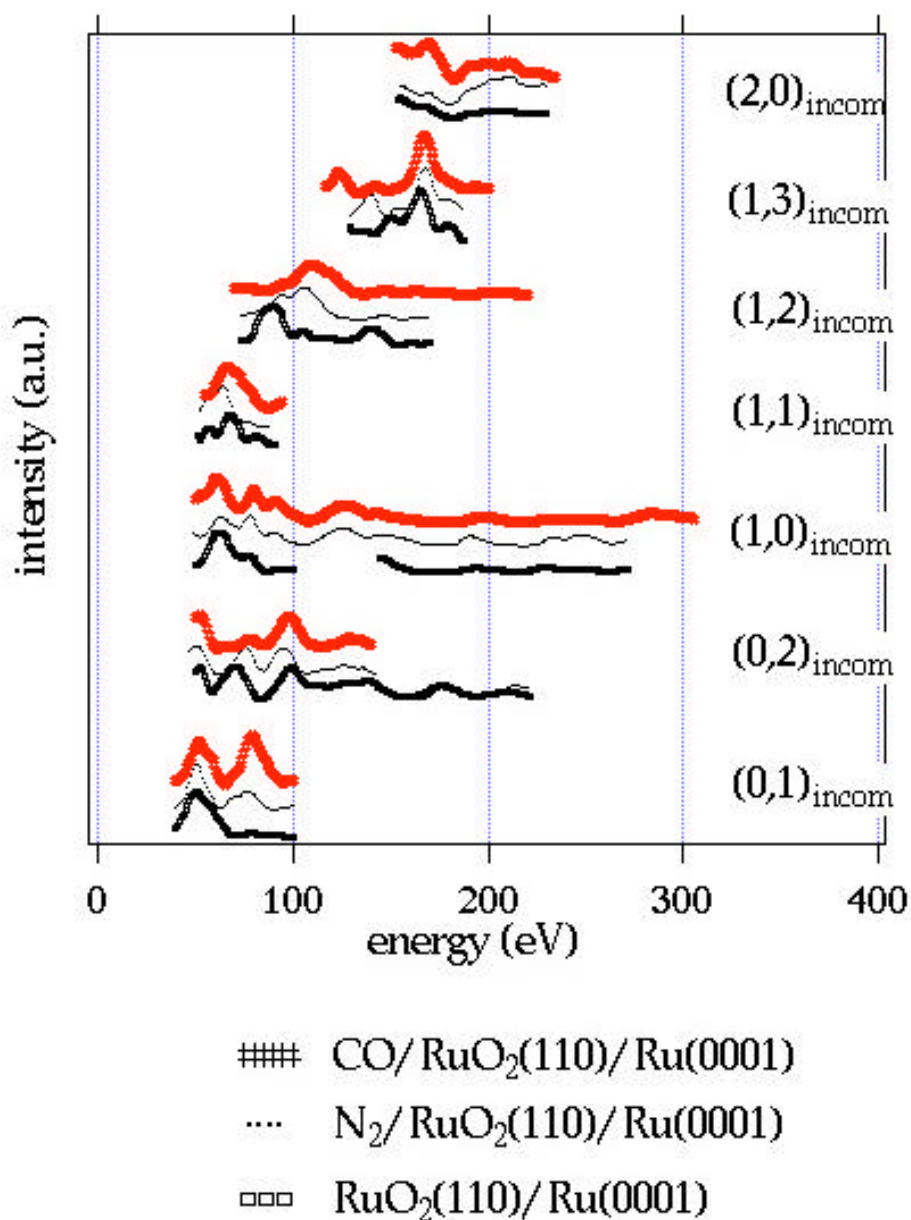


Fig. 4.20. The LEED I/E curves of RuO₂(110)/Ru(0001), N₂/RuO₂(110)/Ru(0001) and CO/RuO₂(110)/Ru(0001) are compared. R_p between RuO₂(110)/Ru(0001) and N₂/RuO₂(110)/Ru(0001) is 0.57, while between N₂/RuO₂(110)/Ru(0001) and CO/RuO₂(110)/Ru(0001) 0.31.

defined adsorption site of N₂. Interestingly, the I/E curves from N₂/RuO₂(110)/Ru(0001) are quite similar to those of CO/RuO₂(110)/Ru(0001). Also on the bare Ru(0001) surface, the I/E curves of ($\sqrt{3}\times\sqrt{3}$)R30°-N₂ turned out to be similar to those of ($\sqrt{3}\times\sqrt{3}$)R30°-CO (R_p = 0.38) [108]. This similarity was supposed to be an

indicative that CO and N₂ occupy the same adsorption site. Due to the small difference in the atomic number of N, C and O, their atomic scattering properties are similar, thus resulting in similar shapes of the I/E curves of CO and N₂ overlayers, as far as their adsorption geometries are similar. Actually, the quantitative I/E analysis disclosed that CO and N₂ position in the same adsorption site on Ru(0001) at a coverage of 0.33 ML, on-top site [108]. Equally, the similarity of the I/E curves of N₂/RuO₂(110)/Ru(0001) and CO/RuO₂(110)/Ru(0001) promises that over RuO₂(110)/Ru(0001), N₂ adsorbs on the same site as CO, on top of cus Ru atom.

In fact, the LEED I/E calculations resulted in an R_p of 0.34 by assuming that N₂ molecules sit vertically above the cus Ru atoms. In these calculations, the Debye temperatures and atomic positions of both N atoms in an N₂ molecule, bridging O, Ru and threefold O in the first main plane and O atoms in the first O bilayer were relaxed in the fit procedure. The atoms in deeper layers were kept at the same positions as in the best-fit structure of RuO₂(110)/Ru(0001). The best-fit structure of N₂ on RuO₂(110)/Ru(0001) is shown in Fig. 4.21. The experimental and the theoretical LEED I/E curves are compared in Fig. 4.22. The distances of N–N and Ru–N are 1.11 Å and 2.06 Å, respectively. These values are comparable to those of the ($\sqrt{3}\times\sqrt{3}$)R30°-N₂ on Ru(0001), where the distances of N–N and Ru–N are 1.10 Å and 2.00 Å, respectively [107].

Comparing the adsorption geometry of N₂ on RuO₂(110)/Ru(0001) to that of CO, the N–N distance (1.11 Å) is slightly shorter than that of C–O (1.13 Å), while the distance of Ru–N (2.06 Å) is longer than that of Ru–C (2.00 Å) by 0.06 Å. In contrast to CO, N₂ is more strongly bound on RuO₂(110)/Ru(0001) than on the bare Ru(0001) surface. The N₂ desorption from RuO₂(110)/Ru(0001) takes place between 110 K and 170 K, while N₂ desorption from Ru(0001) completes below 120 K (Fig. 4.23). This result is consistent with the picture that N₂ is a σ donator, and the cus Ru atoms of the RuO₂(110)/Ru(0001) are more acidic than the Ru atoms on the Ru(0001) surface.

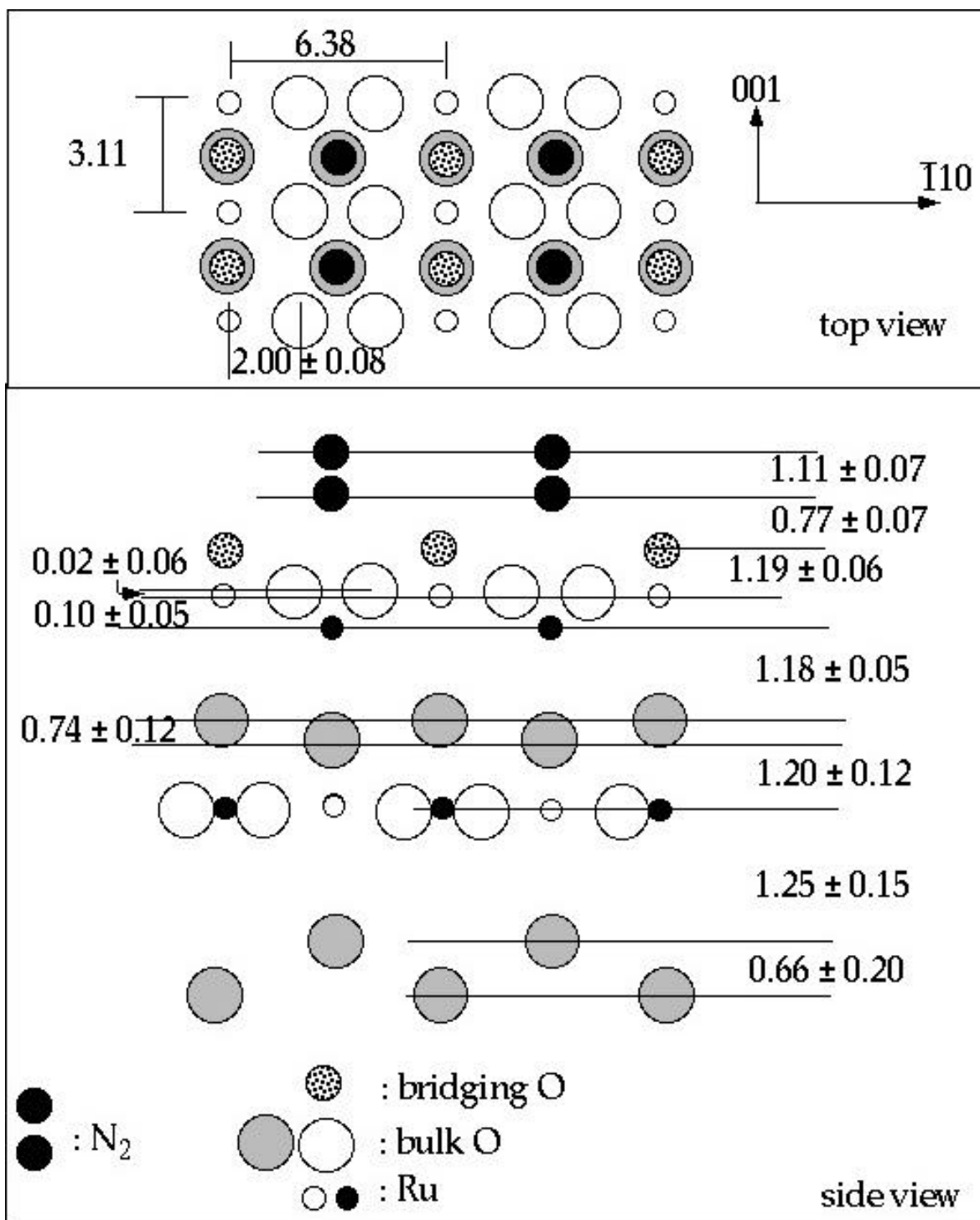


Fig. 4.21. Best-fit structure of N_2 on $RuO_2(110)/Ru(0001)$ determined by LEED I/E calculations. The values are given in Å.

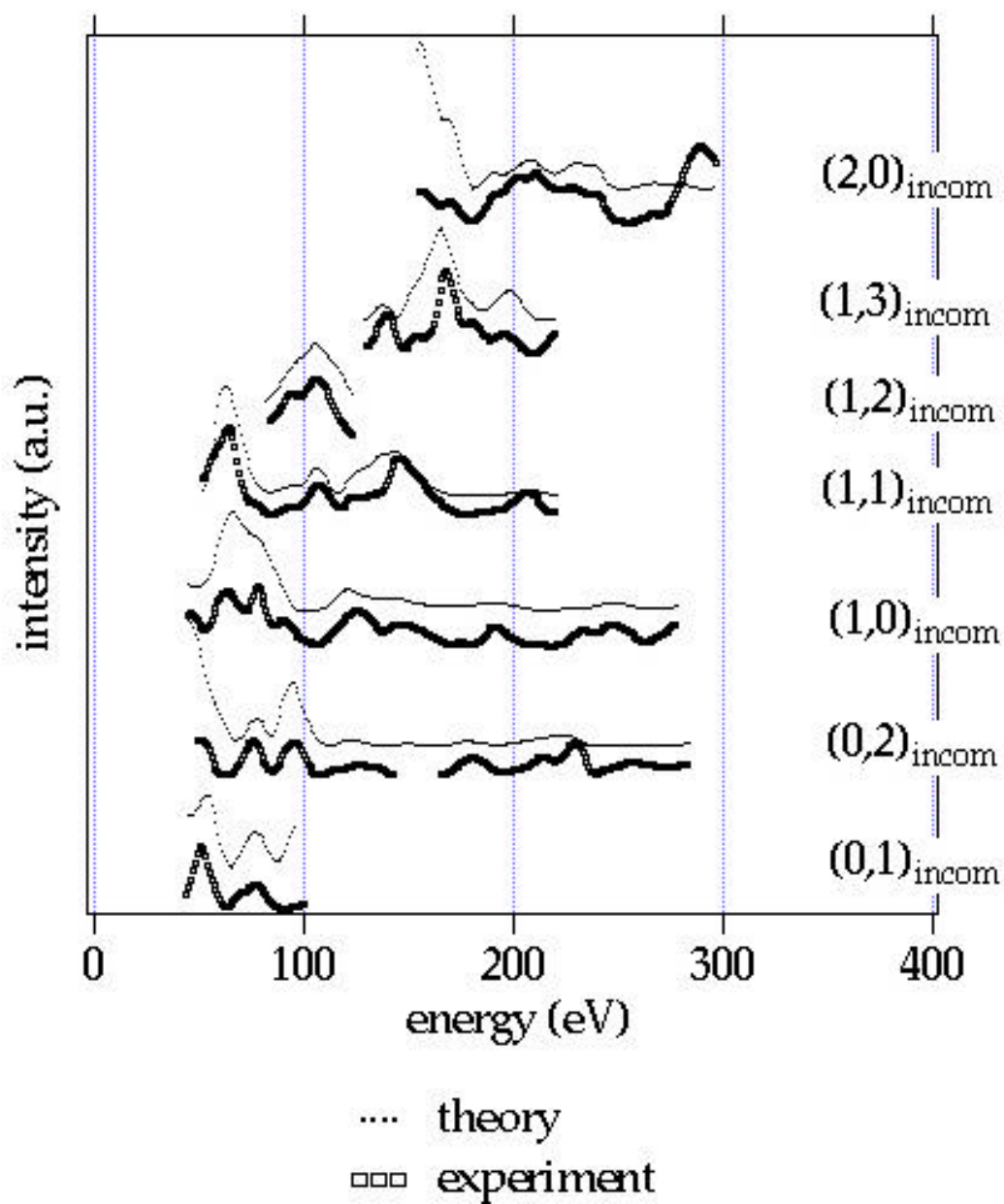


Fig. 4.22. The experimental LEED I/E curves are compared with calculated ones for the best-fit structure of N₂ on RuO₂(110)/Ru(0001) ($R_P = 0.34$).

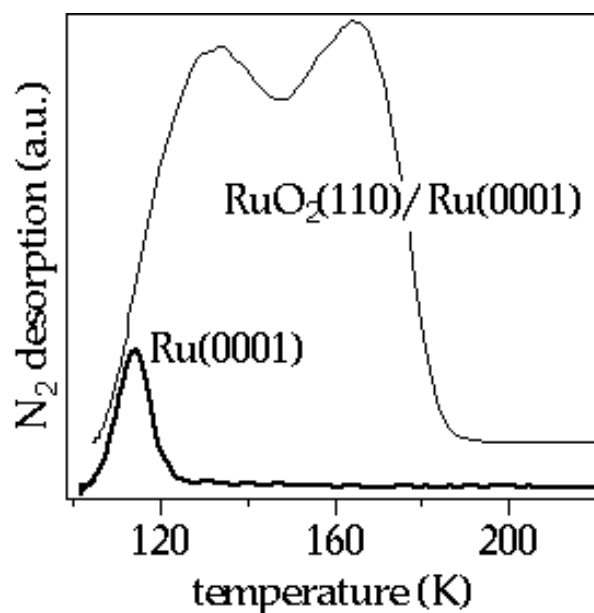


Fig. 4.23. TD spectra of N_2 from $RuO_2(110)/Ru(0001)$ and the bare $Ru(0001)$ surface. 30 L of N_2 was dosed at 110 K. The heating rate was 3 K/s.

4.8 Weakly bound oxygen on $RuO_2(110)/Ru(0001)$

Recently, a new oxygen species was discovered on the O-rich $Ru(0001)$ surface, which desorbs between 350 K and 600 K [109]. The authors of Ref. [109] suggested from isotope exchange experiments that this new oxygen species is dissociatively adsorbed. The probability for a CO molecule to recombine with this weakly bound oxygen to CO_2 is about 20 % at 350 K [109]. The extraordinarily high activity of this species motivated us to investigate the atomic structure of this new oxygen species.

An O-rich $Ru(0001)$ surface showing a LEED pattern as in Fig. 4.2 a) was exposed to O_2 at a sample temperature of 300 K. LEED beam intensities from $(1\times 1)\text{-O}$ and $RuO_2(110)$ patches were measured during O_2 exposures. The I/E curves were collected before and after exposing to O_2 (Fig. 4.24).

The I/E curves of $RuO_2(110)$ change upon O_2 exposures at 300 K. This indicates that the chemisorption of oxygen takes place on $RuO_2(110)/Ru(0001)$. The $(1\times 1)\text{-O}$ related I/E curves do not show any change upon O_2 exposure. The

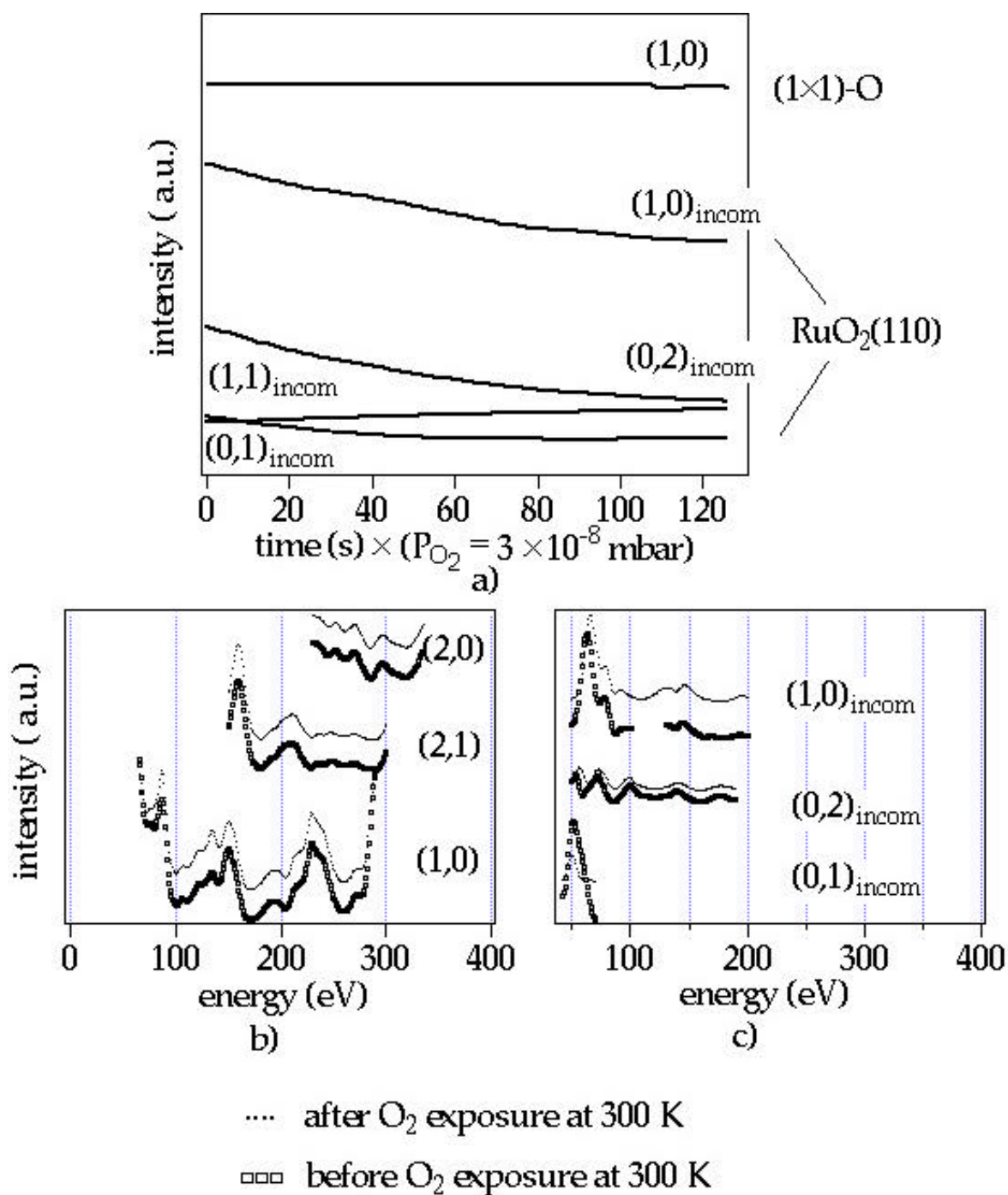


Fig. 4.24. a) The change of the LEED beam intensities of the O-rich Ru(0001) surface during dosing O_2 at 300 K. b) The I/E curves of the $(1 \times 1)\text{-O}$ patches before and after dosing O_2 at 300 K. c) The I/E curves of the $RuO_2(110)$ islands before and after dosing O_2 at 300 K.

changes of the LEED beam intensities in Fig. 4.24 show a similar trend as in the case of CO exposure on the O-rich Ru(0001) surface (Fig. 4.6). Consequently, only the RuO₂(110) islands allow adsorption of oxygen at room temperature, while on the (1×1)-O domains oxygen does not adsorb.

The thermal desorption spectra for various coverages of this weakly bound oxygen are shown in Fig. 4.25. With increasing oxygen coverage, peak temperatures shift to lower temperatures, which is typical for second-order desorption. The results of the thermal desorption experiments and the isotope exchange experiments of Ref. [109] indicate that this oxygen species is atomically adsorbed on the surface.

We discuss the atomic structure of this weakly bound oxygen. On TiO₂(110), moderate O₂ treatment at 500 K led to a surface reconstruction ('rosette' structure) as identified by STM [110]. We did not observe any indication of a surface reconstruction by exposing RuO₂(110)/Ru(0001) to O₂ at 300 K with LEED.

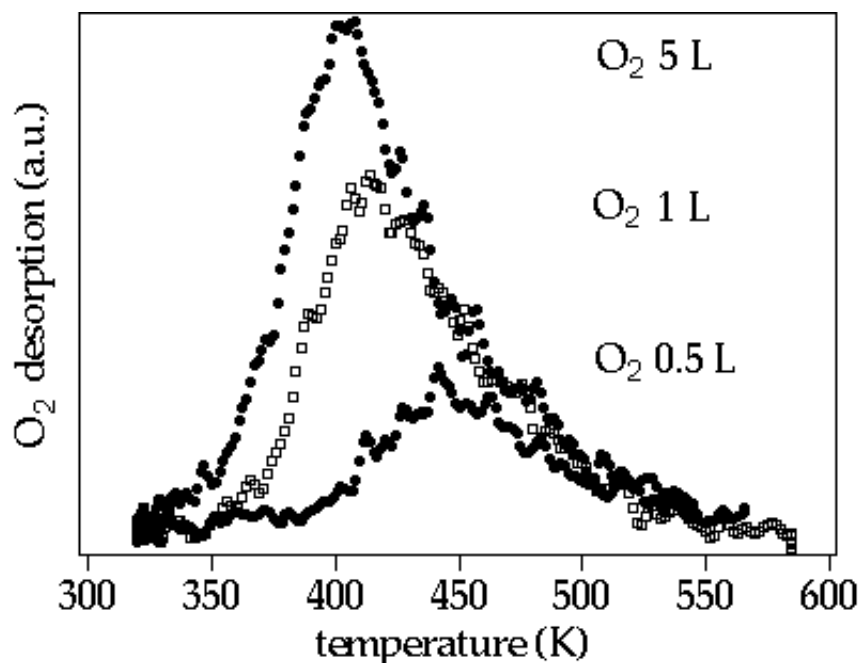


Fig. 4.25. TD spectra of the weakly bound oxygen on RuO₂(110)/Ru(0001). O₂ was dosed at 300 K. The amounts of O₂ doses are given. The heating rate is 3 K/s.

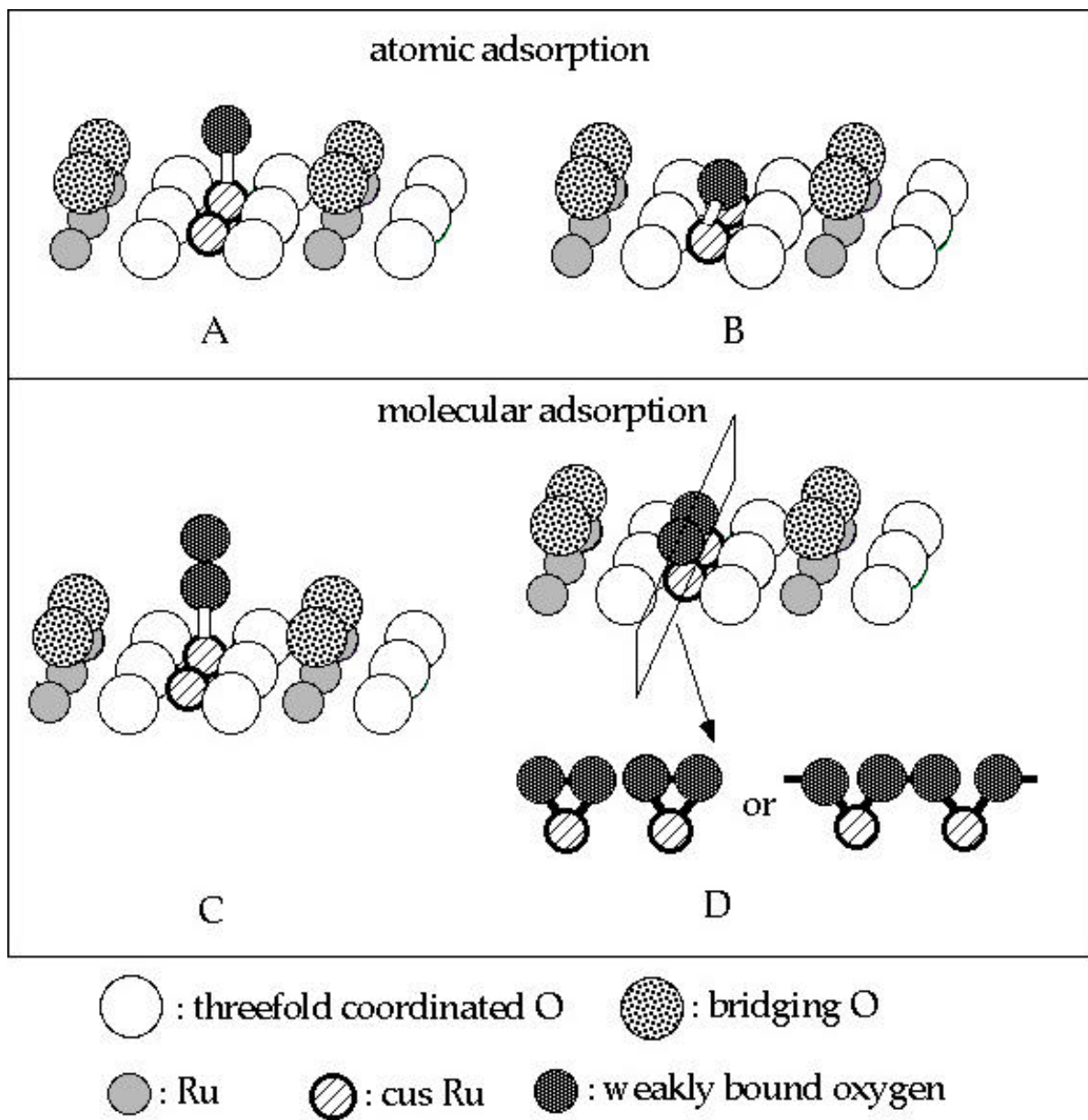


Fig. 4.26. Possible adsorption geometries of the weakly bound oxygen species on $\text{RuO}_2(110)/\text{Ru}(0001)$. a) Atomic O on top of cus Ru atom. b) Atomic O on bridge site. c) O_2 attaching one O atom to a cus Ru atom. d) O_2 lying down.

Taking into account that no surface reconstruction is induced by the adsorption of weakly bound oxygen, there are two possible adsorption geometries for additional O atoms on RuO₂(110)/Ru(0001): O atoms sit in on-top positions or in bridge positions (Fig. 4.26 A and B).

The distance between the additional O atom in the bridge position (coordinating to two cus Ru atoms) and the three fold coordinated O in the first (Ru+O) plane is just 1.6–1.7 Å, assuming that the Ru–O bond length should not exceed 2.1 Å. The mean distance between lattice O atoms in RuO₂ is 2.4 Å. A distance of 1.6 Å between two atomic O is therefore too short, considering the repulsive interaction between O atoms. On RuO₂(110)/Ru(0001), therefore, the on-top sites (Fig. 4.26A) are more probable than the bridge sites for O atoms (Fig. 4.26B).

The experimental data set, which was collected after exposing ‘3 L’ of O₂ to RuO₂(110)/Ru(0001) at 300 K, contains I/E curves from seven symmetrically different beams with the total energy range of 950 eV. Two adsorption sites, on-top

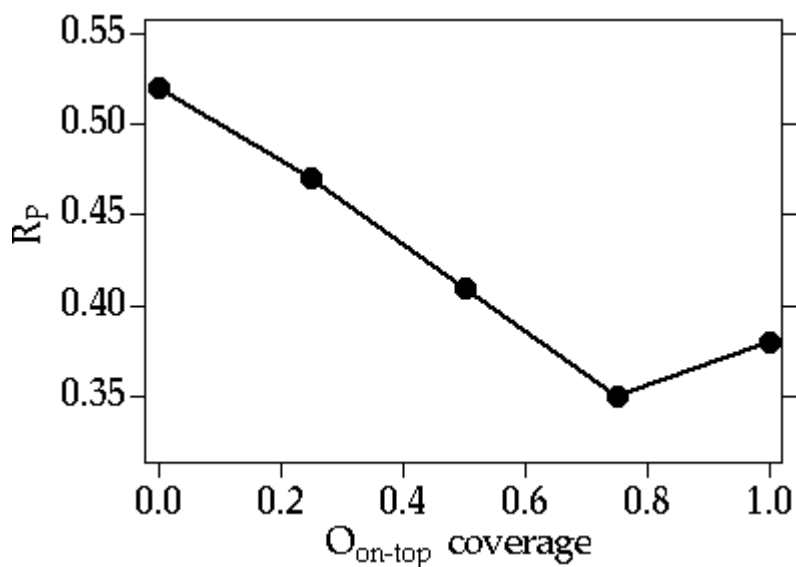


Fig.4.27. Change of R_p depending on the O_{on-top} coverage in the I/E calculations.

and bridge sites were tested in LEED I/E calculations. In these calculations, the Debye temperatures and atomic positions of the weakly bound O, bridging O, Ru and threefold O in the first main plane and the O atoms in the first O bilayer were released in the fit procedure. The atoms in deeper layers were kept at the same positions as in the best-fit structure of RuO₂(110)/Ru(0001).

The calculations with various coverages of the on-top O were carried out, whose results are summarized in Fig. 4.27. The agreement between theoretical and experimental I/E curves improves significantly, when the on-top O is included in the model. The optimum concentration of on-top O is 75 ± 25 % ($R_p = 0.36$). The model with the bridge site results in $R_p = 0.46$. The best-fit structure for the on-top O on RuO₂(110)/Ru(0001) is presented in Fig. 4.28. The calculated and the experimental LEED I/E curves for this structure are reproduced in Fig. 4.29.

Comparing the structure of O/RuO₂(110)/Ru(0001) to that of RuO₂(110)/Ru(0001), the Ru is lifted upwards by 0.19 Å with respect to the other Ru in the same plane by on-top O. This can be explained by the electron withdrawing nature of the atomic O. O atoms accept electrons from the bonding band of substrates so that the bonding between substrate atoms becomes weaker. The bond length of Ru–O_{on-top} is 1.77 Å, which is markedly shorter than the bulk value, 1.91 Å.

We also found a supporting evidence for the existence of the on-top O from the investigations of the (N₂ + weakly bound O) coadsorption system. On the RuO₂(110)/Ru(0001) surfaces precovered with different coverages of the weakly bound oxygen, 30 L of N₂ was postdosed at 110 K. Subsequently, thermal desorption experiments of N₂ and O₂ were carried out (Fig. 4.30). N₂ coverage decreases gradually with increasing coverage of the weakly bound O, which indicates that the weakly bound oxygen inhibits the adsorption of N₂ at 110 K. Apparently, the weakly bound oxygen favors the same adsorption site as N₂, i.e., on-top site. At the saturation coverage of weakly bound O, just 25 % of N₂ with respect to its saturation coverage can be adsorbed.

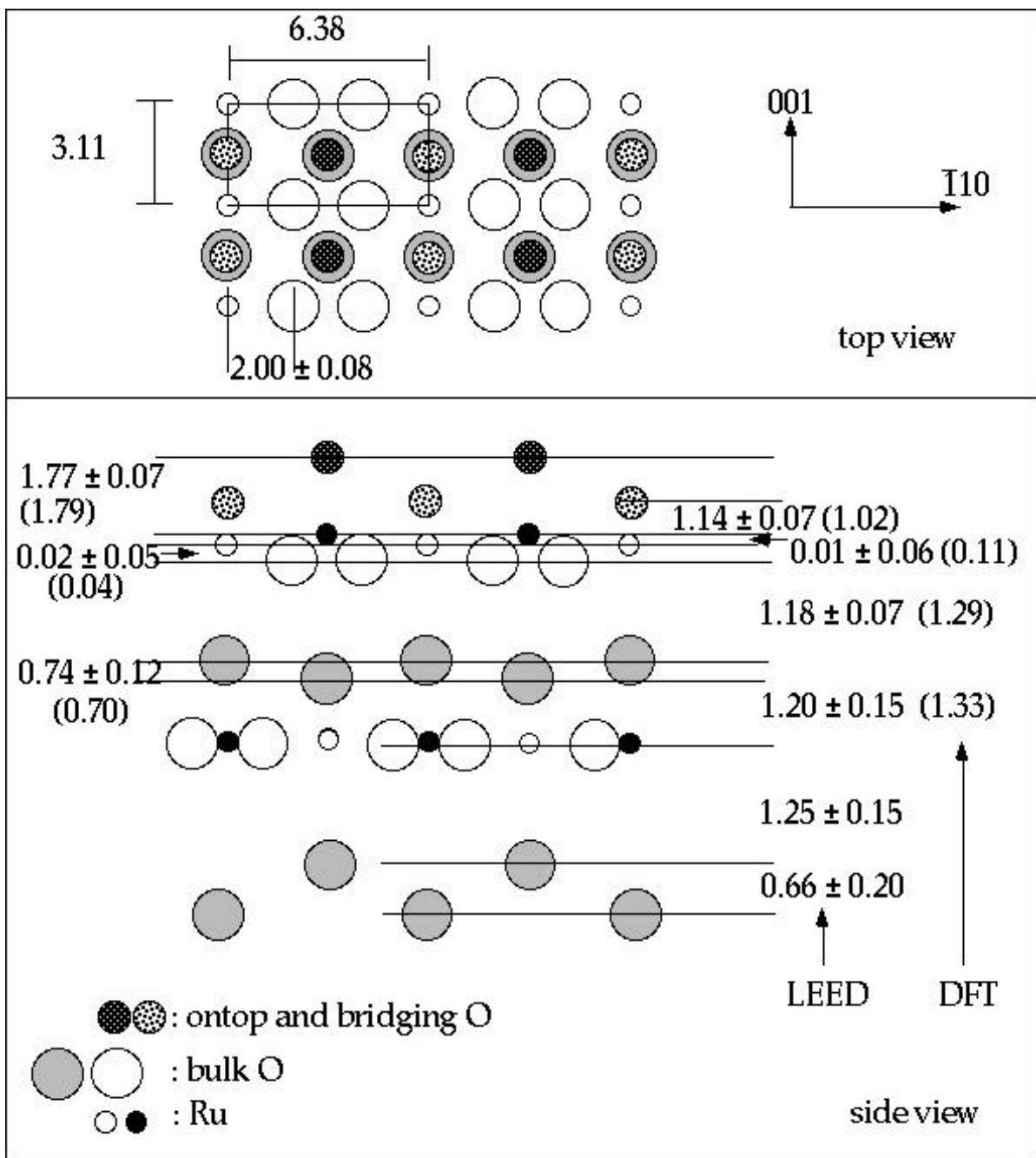


Fig. 4.28. Best-fit structure of the on-top O over RuO₂(110)/Ru(0001) determined by LEED I/E calculations and DFT calculations. The values are given in Å.

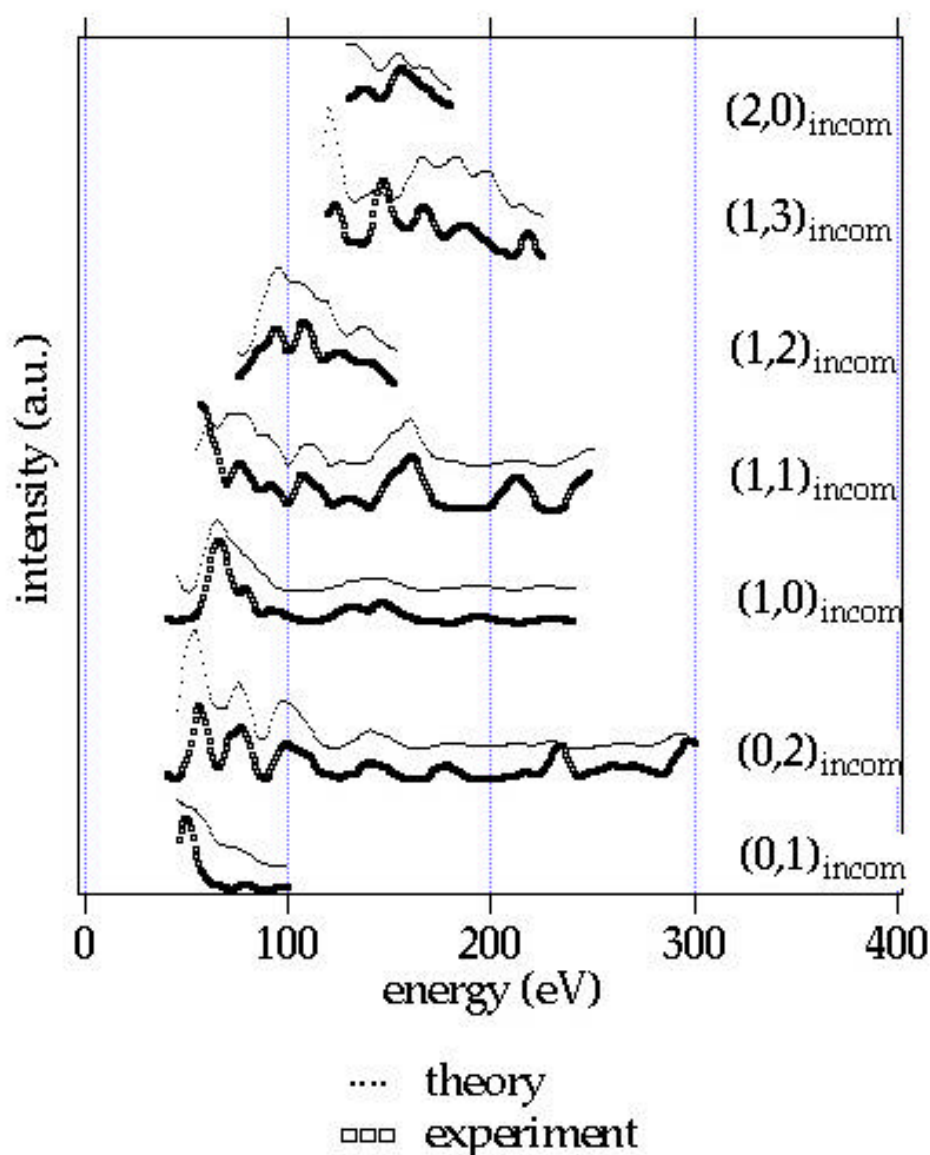


Fig. 4.29 The experimental LEED I/E curves are compared with calculated ones for $O_{\text{on-top}}/\text{RuO}_2(110)/\text{Ru}(0001)$ ($R_p = 0.36$).

The results of DFT calculations for $\text{RuO}_2(110)/\text{Ru}(0001)$ and $\text{CO}/\text{RuO}_2(110)/\text{Ru}(0001)$ are in excellent agreement with experimental results. However, the results of DFT calculations for the on-top O [111] are contradictory to those of the experiments.

The adsorption energy of the on-top O estimated by DFT calculations is smaller than 0.2 eV with respect to the half energy of an $\text{O}_2(\text{g})$ molecule [111]. The desorption temperature of O_2 from $\text{RuO}_2(110)/\text{Ru}(0001)$ is between 350 K and 600K,

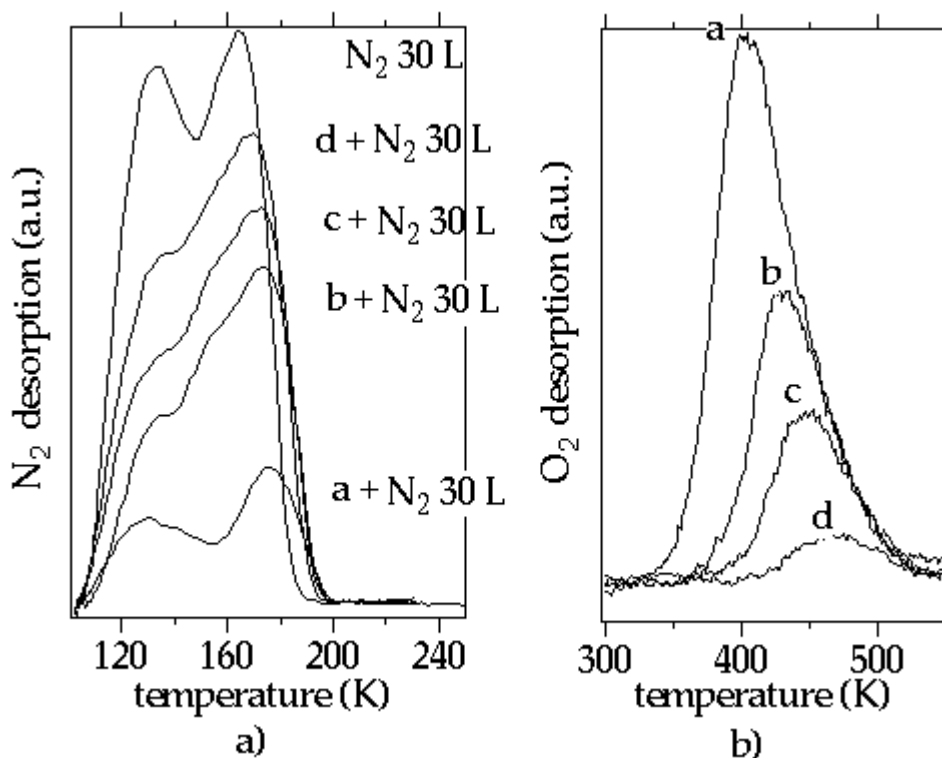


Fig. 4.30. TD spectra of N_2 (a) and O_2 (b) from the (weakly bound $O+N_2$) coadsorption system on $RuO_2(110)/Ru(0001)$. After the weakly bound oxygen species with various coverages (a to d) had been prepared by dosing '3 L' of O_2 at 300 K and subsequent heating to a) 300 K, b) 360 K, c) 375 K, d) 400 K, 30 L of N_2 was given at 110 K. The heating rate is 3 K/s.

which indicates the activation energy for the associative desorption of two O atoms to O_2 to be higher than 1.0 eV. As it is illustrated in Fig. 4.31, the total activation barrier for an associative desorption is the sum of the binding energy of two atomic O ($2E_b$) on the surface and an additional activation barrier (diffusion barrier, E_a). The only way to rationalize the O_2 desorption temperature between 350 K and 600 K with a binding energy of an atomic O below 0.2 eV is that E_a should be higher than 0.6 eV. However, the experimentally determined sticking probability of O_2 on $RuO_2(110)/Ru(0001)$ at 300 K is substantially high (Sticking coefficient $S_o = 0.8$), indicating quite low E_a [109]. Essentially, the binding energy of the weakly bound O (E_b) on $RuO_2(110)/Ru(0001)$ should be larger than 0.5 eV, which is contradictory to the result of DFT calculations.

Besides the binding energy of the on-top O, structural parameters from DFT and

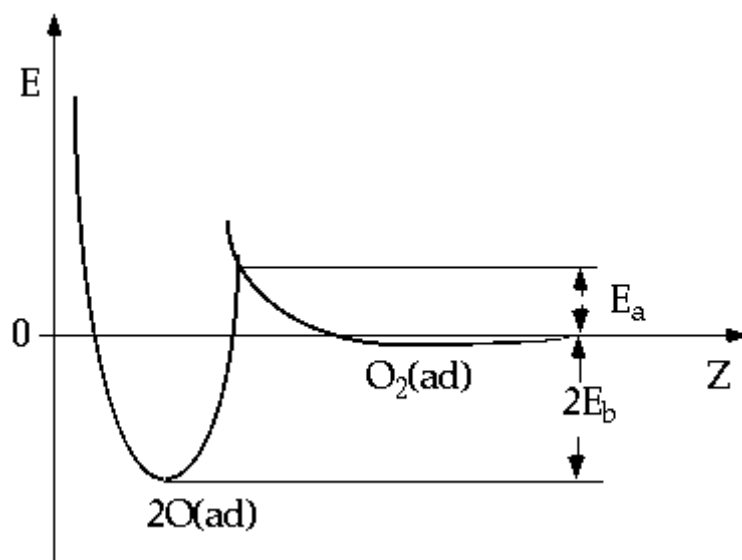


Fig. 4.31. One-dimensional potential energy diagram of dissociative adsorption of O_2 involving activation barrier of E_a . E_b is the binding energy of an atomic O with respect to the half energy of an $O_2(g)$ molecule.

LEED do not agree very well (Fig. 4.28). Especially, the atomic position of Ru attaching to the on-top O determined by DFT and LEED is conflicting.

Because of the unsatisfactory agreement between DFT calculations and experimental results, we carried out the quantitative LEED I/E calculations with the models involving molecular oxygen instead of atomic O on $RuO_2(110)/Ru(0001)$. Two models, O_2 molecules bound vertically (Fig. 4.27 C) or laterally (Fig. 4.27D) on the cus Ru atoms, were tested. In the model of Fig. 4.27D, two different configurations can be considered. An O_2 molecule lying parallel to the surface can be coordinated to one or two cus Ru atoms. LEED is not very sensitive to lateral displacement. Thus, these two species with different bonding configuration cannot be discriminated with LEED. Note that in Fig. 4.26D, the O–O bond length should be about 1.5 Å, while for Ru–Ru 3.11 Å.

The models with adsorbed molecular oxygen (Fig 4.26 C and D), however, gave worse agreements between theory and experiment in the LEED I/E calculations than that of on-top atomic O ($R_p = 0.52$ for model C and $R_p = 0.45$ for D).

Thermal desorption experiments including isotope exchange experiments [109],

thermal desorption experiments of (N_2 + weakly bound oxygen) coadsorption systems, and the LEED I/E simulations for a number of models illustrated in Fig. 4.26 were carried out to characterize the weakly bound oxygen on the atomic scale. The new oxygen species is in an atomic state and is adsorbed above the cus Ru atoms. However, the results of DFT calculations do not agree with these experimental results.

4.9 O-rich-phases without oxide formation

In Fig. 4.32, TD spectra of the O-rich phases prepared in various ways are shown.

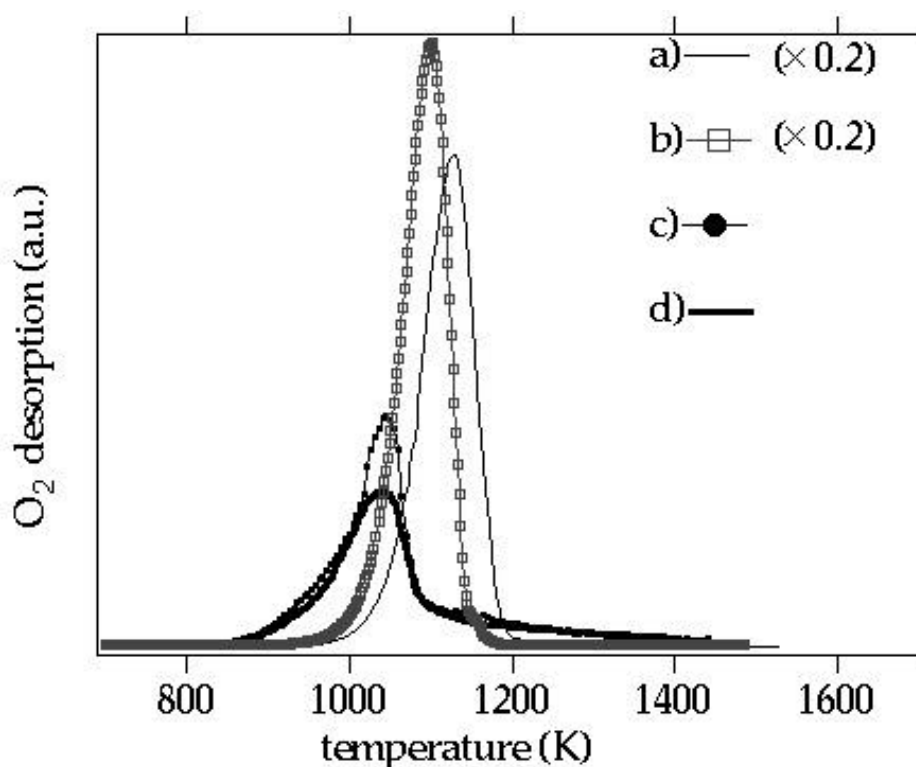


Fig. 4.32. TD spectra of O-rich phases prepared by various methods: a) ‘60000 L’ of O_2 at 1050 K, b) ‘60000 L’ of O_2 at 950 K, c) 500 L of NO_2 at 600 K, d) ‘60000 L’ of O_2 at 600 K. The quotation marks indicate that the shower system was used for dosing and amounts of exposures were estimated by reading background pressures during exposures. $RuO_2(110)$ is identified with the LEED pattern for d), while the LEED patterns of a) and c) exhibit the (2×2) and the (1×1) structure, respectively. No LEED pattern is visible for b). The heating rate was 3 K/s.

$\text{RuO}_2(110)$ is formed by exposing $\text{Ru}(0001)$ to large amounts of $\text{O}_2(\text{g})$ ('60000 L') at sample temperatures between 600 K and 800 K. In the TD spectrum (Fig. 4.32d), the main desorption peak is at about 1050 K. Heating the surface to 1050 K, therefore, removes most of oxygen, and only about 0.75 ML of chemisorbed O atoms are left on the surface. LEED indicated a (2×2) pattern without any traces of LEED spot characteristics for $\text{RuO}_2(110)$. In other words, upon annealing the $\text{Ru}(0001)$ surface to 1050 K, the $\text{RuO}_2(110)$ domains decompose, and only chemisorbed O atoms are left on the surface. A quite similar behavior was reported for bulk RuO_2 surfaces. Annealing bulk RuO_2 in UHV at about 1000 K changes the composition at the surface in a way that the oxide is replaced by a metallic Ru slab on which O atoms are chemisorbed [112].

If the O-rich phase is prepared at 950 K with an O_2 exposure of '60000 L', the O coverage is about 30–50 ML (this preparation procedure revealed a poor reproducibility). After exposing this O-rich $\text{Ru}(0001)$ surface to CO at 120 K, the CO and CO_2 signals were detected between 200 K and 600 K in a thermal desorption experiment (Fig. 4.33.) CO is strongly bound on this phase, and CO can recombine with O atoms from this O-rich phase to CO_2 . According to the molecular beam experiments, the CO to CO_2 conversion probability of the O-rich phases prepared between 800 K and 1000 K is about 1 %. [113]. Based on the high activity towards CO oxidation, we suggest that this phase be covered by a disordered or rough RuO_2 film.

Another route to synthesize O-rich $\text{Ru}(0001)$ surfaces is to expose the $\text{Ru}(0001)$ surface to high doses of O_2 ('60000 L') at a sample temperature of 1050 K. This procedure results in a surface structure exhibiting a (2×2) LEED pattern. However, the total O uptake was equivalent to 30–50 ML (Fig. 4.32a)). Again, the resulting O uptake revealed a poor reproducibility. The same preparation was recently applied by Böttcher et al. [113], who found that the resulting surface is virtually inactive in oxidizing CO molecules. They interpreted this surface in terms of an inactive RuO_2 film [113]. As outlined above, RuO_2 decomposes around 1000 K.

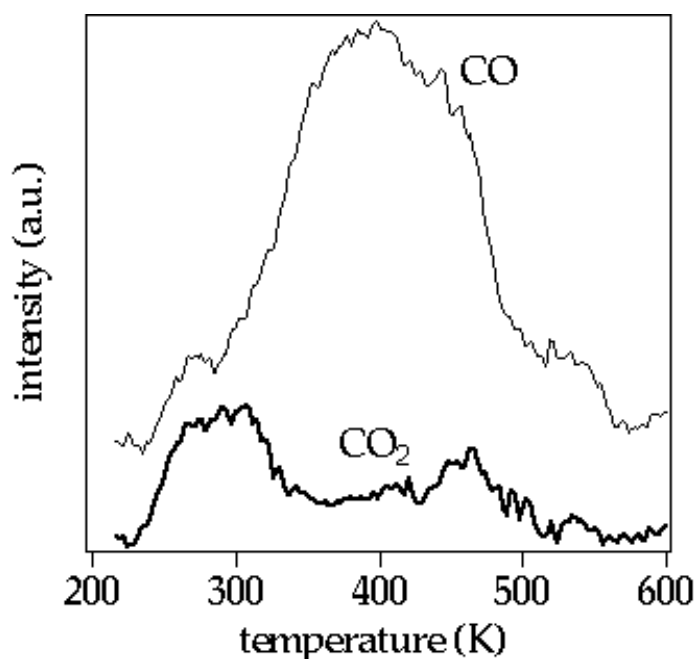


Fig. 4.33. CO and CO₂ desorption from the O-rich phase prepared by '60000 L' of O₂ at 950 K followed by exposing 30 L of CO at 120 K. The quotation marks indicate that the shower system was used for dosing and amounts of exposures were estimated by reading background pressures during exposure.

Preparation at 1050 K is therefore expected to give a Ru surface with chemisorbed O and additional O atoms eventually dissolved in the bulk.

In Fig. 4.34, we reproduced the LEED I/E curves of the O-rich phase prepared by O₂ at 1050 K. These I/E curves are identical to those of the pure (2×2)-3O overlayer with an O coverage of 0.75 ML. This suggests that the surface structure is identical. Substantial amounts of subsurface O atoms in the near-surface region could not be identified.

An alternative way to produce O-rich phases is using NO₂ as a source of atomic O. The Ru(0001) surface is exposed to high doses (500 L) of NO₂ instead of molecular oxygen, keeping the sample temperature at 600 K. The O₂ TD spectrum is overlaid in Fig. 4.32c). From this spectrum, the total amount of O was estimated to be about 5 ML. Quite surprisingly, the LEED pattern still exhibited only spots

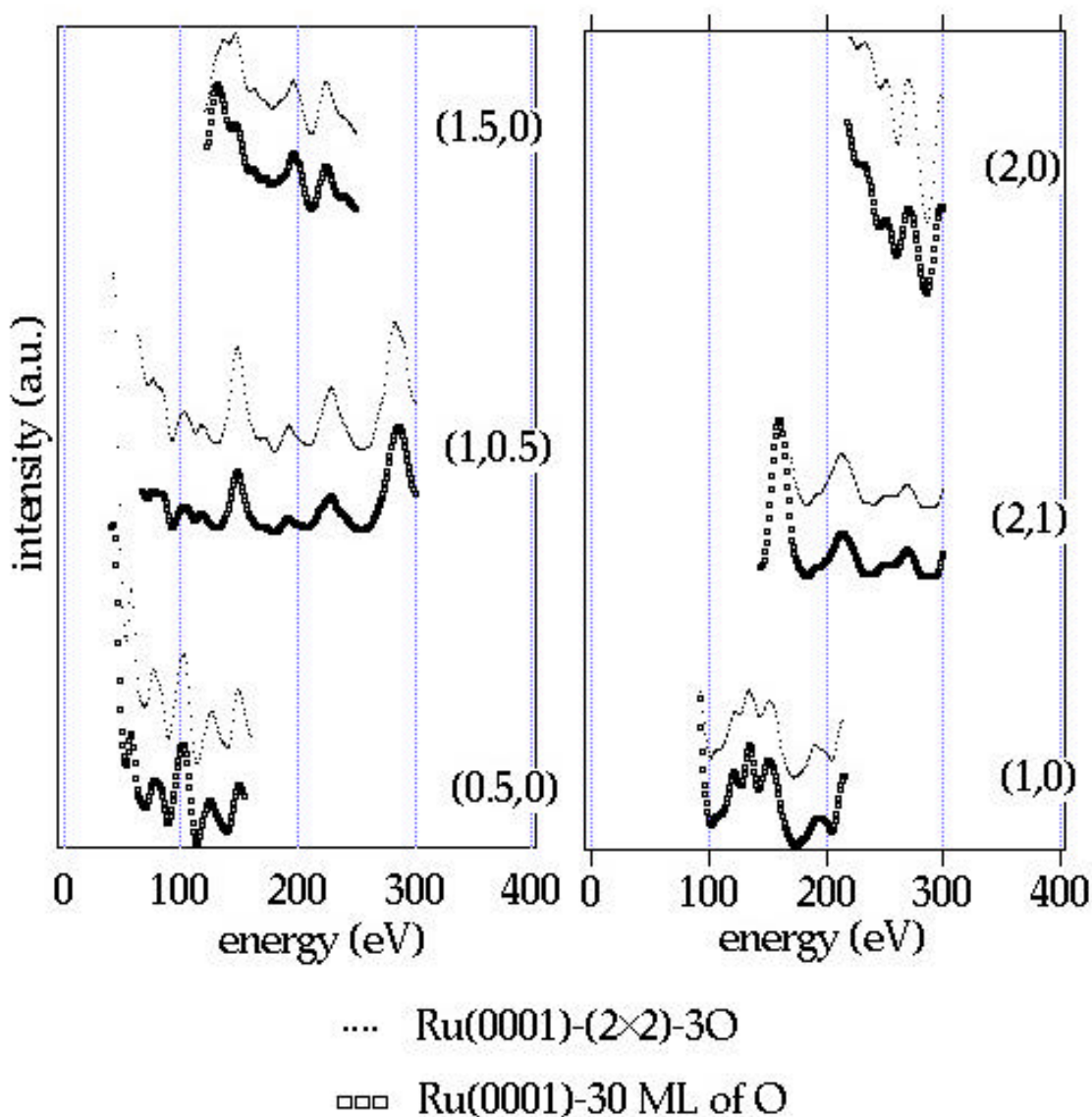


Fig. 4.34. The LEED I/E curves of the O-rich phase prepared by O_2 exposure of '60000 L' (quotation marks indicate that gas shower were used for dosing and the doses was recorded by ion-gauge reading) at a sample temperature of 1050 K with an O coverage of about 30–50 ML. The LEED pattern indicates a (2×2) -structure. For comparison, the I/E curves of the well-defined (2×2) -3O overlayer at an O coverage of 0.75 ML are shown. The Rp between these two data sets is 0.05.

from the (1×1) -O structure, but no indications for the formation of RuO_2 patches. Only by dosing even more NO_2 , it was eventually possible to prepare an O-rich phase with a LEED pattern identical to Fig. 4.2 a. At the time the paper on the

titration experiments over O-rich Ru(0001) was published [23], it was assumed that NO₂ and O₂ exposures lead to identical surface structures, as long as the O load is the same. Accordingly, the (1×1)-O overlayer in combination with dissolved O (albeit erroneously) was considered as the active phase. The actual titration experiments [23] were, however, carried out with an O-rich Ru(0001) surface, prepared with O₂ at sample temperatures between 600 K and 800 K.

In Fig. 4.35, we compare the LEED I/E curves of the (1×1) spots obtained after the O-rich phase was prepared with 500 L of NO₂ at a sample temperature of 600 K with those of a well-defined (1×1)-O surface (the total amount of O was 1 ML as estimated by TDS). The striking similarity of both LEED data sets implies immediately that also the atomic geometries are identical. This means that this O-rich phase consists of an (1×1)-O overlayer. A concentration of subsurface O of more than 10 % between the top three Ru layers could be excluded from a previous analysis [25, 26]. Obviously, the O atoms in excess of 1 ML are not visible in LEED and are hence likely to be dispersed across deeper layers.

We observed large amounts of oxygen incorporating into the bulk by exposing O₂ at 1050 K. This result may indicate that the equilibrium concentration of O in Ru may be substantially high at 1050 K due to the large solubility of O in Ru at this temperature range. Upon rapid cooling the sample, one may expect that O atoms dissolved in the Ru bulk at higher temperatures should be released back into the gas phase, because the solubility of O in Ru should decay while cooling the sample.

However, the diffusion rate of oxygen in the metal phase declines with decreasing temperature. Assuming that D_O is 9.3 cm²/s and activation energy (E_a) is 78 kcal/mol for O diffusion (this value was reported for Pt [114], diffusion constant $D = D_O \exp(-E_a/RT)$), one can estimate an average time (t) for oxygen to diffuse along a given distance by using the formula of random walk displacement

$$x = 2(Dt)^{1/2} . \tag{4.9.1}$$

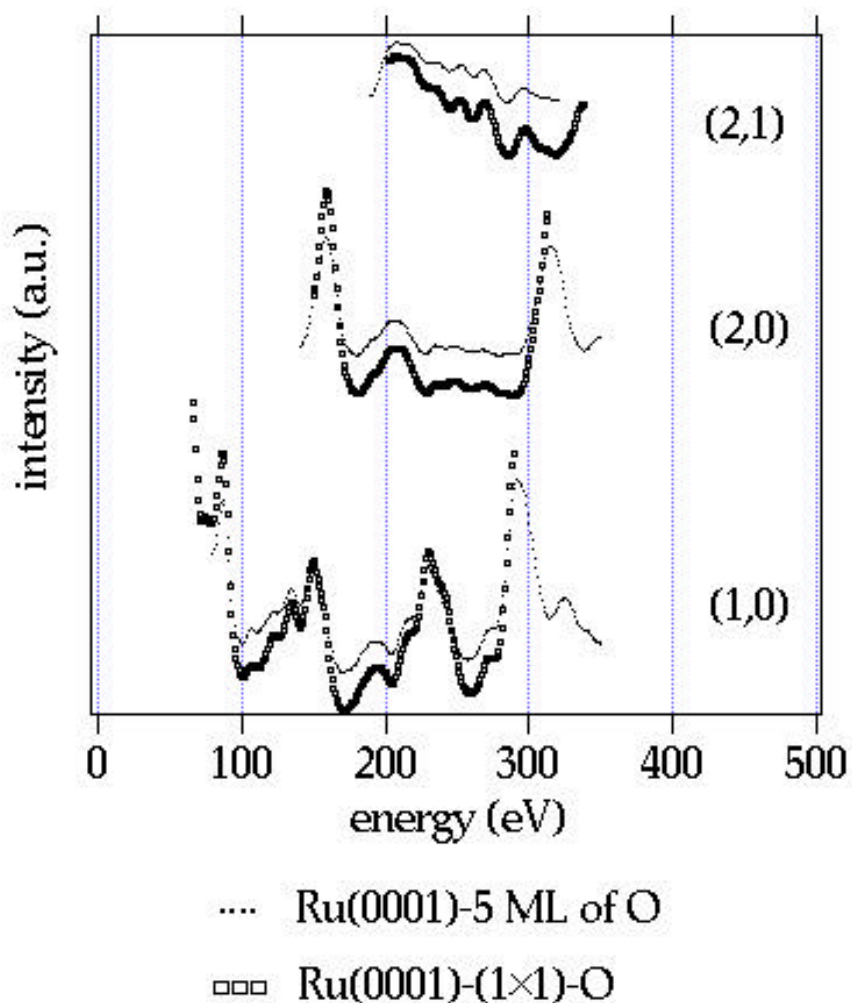


Fig. 4.35. The LEED I/E curves of the O-rich phase prepared by an $\text{NO}_2(\text{g})$ exposure of 500 L at a sample temperature of 600 K. The O coverage is about 5 ML, showing only a (1×1)-pattern. The I/E curves of the (1×1)-O at the O coverage of 1.0 ML are also shown. The R_p between these two data sets is 0.06.

It takes 2×10^{-4} s at 1473 K, but 10^5 years at 573 K for oxygen to cross 20 Å in Pt [114].

When the bare Ru(0001) is exposed to O_2 at 1050 K, large amounts of oxygen are able to penetrate into the bulk because of a substantially high equilibrium oxygen concentration. Subsequent cooling may freeze oxygen in the metal phase due to the reduced diffusion rate of oxygen at lower temperatures.

Summarizing this chapter, our results show that there are no subsurface O atoms detectable with LEED. The existence of the O atoms in the deeper layers were identified by thermal desorption spectra. The catalytic activity of O-rich Ru(0001) is quite low, when no RuO₂ is formed. Only RuO₂ is a catalytically active species of O-rich phases of Ru(0001).